行政院國家科學委員會補助專題研究計畫 ■成果報告
□期中進度報告

新型三階濾波天線之研究與開發

計畫類別：■個別型計畫　□整合型計畫
計畫編號：NSC97-2221-E-009-041-MY3
執行期間：97 年 8 月 1 日至 100 年 7 月 31 日

執行機構及系所：國立交通大學電信工程研究所

計畫主持人：鍾世忠
計畫參與人員：莊肇堂

成果報告類型(依經費核定清單規定繳交)：□精簡報告　■完整報告

本計畫除繳交成果報告外，另須繳交以下出國心得報告：
□赴國外出差或研習心得報告
□赴大陸地區出差或研習心得報告
□出席國際學術會議心得報告
□國際合作研究計畫國外研究報告

處理方式：除列管計畫及下列情形者外，得立即公開查詢
■涉及專利或其他智慧財產權，□一年■二年後可公開查詢

中　華　民　國　100　年　8　月　30　日

CONTENTS

摘要

摘要—本計劃旨在研究具有高頻帶邊緣選擇之新型縮小化濾波天線，包含超寬頻天線以及高整合度模組兩方面的應用。本計劃所提出的天線設計，均具備結構簡單、製作與積體化容易、成本低廉，以及展現良好的濾波器響應。首先, 提出兩種小型的耦合共振器。所設計之新型耦合線共振器，其在濾波天線中可產生一對可調整頻率的傳輸零點。此外，耦合開路/短路殘斷共振器在具有頻帶截止功能之超寬頻天線設計中，呈獻一個傳輸零點於中心頻率以及一對可調整頻率的傳輸極點於帶通頻段。所設計的兩種共振器皆可達到高裙帶選擇於頻帶轉換區域。

亦提出多種新型印刷式濾波天線之合成與設計。首先建立倒 L 型與倒 F 型天線之等效電路模型，其主要為串聯 RLC 共振型電路，並利用與全波模擬結果比較，進行天線之等效電路成分萃取。此兩種天線在本研究除了當做主要輻射體，亦是帶通濾波器中最後一階共振器。為了達到有效整合與簡單設計之要求，提出共同設計之方法來整合濾波器與天線。以印刷式倒 L 型天線與平行耦合微帶線為例，設計與合成一帶通濾波天線。接著提出具有高頻帶邊緣選擇之印刷式濾波天線，其使用與傳統天線相同電路基板面積。所提出的架構不僅是一個輻射體，亦是一個二階帶通濾波器，其中濾波器的一階由天線提供，而另一階由耦合線共振器提供。透過耦合線共振器之設計，在截止頻帶可產生兩個可調的傳輸零點，可達到高頻帶邊緣選擇。而為了縮小電路面積與寄生的輻射效應，提出縮小化耦合線共振器，其利用微帶線、共平面波導之結構與側面耦合之方法來實現，並嵌入於Γ型與倒 F 型天線面積中。根據濾波器的規格，詳細提出濾波天線的設計步驟。與單一天線做比較，所提出之濾波天線除了具有與單一天線近似的天線增益外，亦呈獻較佳的天線增益頻帶邊緣選擇及平緩天線增益響應於帶通頻段。

最後，提出高截止頻帶邊緣選擇之具頻帶截止功能的超寬頻天線設計。所提出的天線包含一個輻射貼片與嵌入式二階帶拒濾波器.使用與典型 UWB 天線相同的電路基板面積，將非均勻式短路殘斷與耦合開路/短路殘斷共振器所組成之帶拒濾波器設計於傳統天線中。以操作頻率為 5.5GHz 且具最大平坦響應之帶拒濾波器為規格，對於所設計之天線提出詳細的設計步驟。與傳統的天線比較，所提出的 UWB 天線在頻段 5.15GHz 與 5.95GHz 之間具有良好的截止頻帶抑制。所提出之架構可達到高頻帶邊緣選擇與平坦的折返損耗於截止頻帶中。所量測之結果與設計的做比較，包括折返損耗、全輻射功率、天線增益，具有良好的一致性。

關鍵字—頻帶邊緣選擇，濾波天線，殘斷共振器，耦合線共振器、超寬頻天線、全輻射功率。

ABSTRACT

Abstract—This project is focused on the design of the novel compact filtering antennas with high band-edge selectivity. These antenna designs have the merits of simple in geometry, easy for manufacture and integration, low-cost, and exhibits good filter frequency responses. First, two kinds of compact coupled resonators are proposed. The new coupled line resonator in the filtering antenna can provide one pair of transmission zeros with tunable frequencies. Also, the coupled open-/short-circuited stub resonator in the band-notched UWB monopole antenna can exhibit a transmission zero at the center frequency and a pair of transmission poles with tunable frequencies at the two sides. Both of these two resonators can achieve high skirt selectivity in the band transition region.

Secondly, the synthesis and design of the new printed filtering antennas are presented. The equivalent circuit models for the inverted-L and -F antennas, which are mainly a series RLC circuit, are first established. The values of the corresponding circuit components are then extracted by comparing with the full-wave simulation results. These two antennas here perform not only a radiator but also the last resonator of the bandpass filter. For the requirements of efficient integration and simple fabrication, the co-design approach for the integration of filter and antenna is introduced. The printed inverted-L antenna and the parallel coupled microstrip line sections are first used for example to illustrate the synthesis of a bandpass filtering antenna. Moreover, the compact printed filtering antennas with high band-edge gain selectivity are presented simultaneously. Occupying about the same substrate area as a conventional antenna, the proposed structure not only serves as a radiator but also a second-order bandpass filter, with one filter pole provided by a antenna and the other by a the proposed coupled line resonator. High band-edge selectivity is achieved due to two additional stop-band transmission zeros provided by the coupled line resonator. To minimize the required area and reduce the spurious radiation, a coupled line structure composed of a microstrip line and a coplanar waveguide by broadside coupling is adopted and intruded into the Γ-shaped and inverted- F antenna areas. The design procedures are given, which clearly indicates the steps from the filter specifications to the implementation. As compared to the conventional antennas, the proposed filtering antennas not only possesses a similar antenna gain but also provides better band-edge gain selectivity and flat passband gain response. The measured results, including the S-parameters, total radiated power, and antenna gains versus frequency, have good agreement with the designed ones.

Finally, a novel design of band-notched ultra-wide-band (UWB) monopole antenna with high notch-band-edge selectivity is proposed. The proposed antenna consists of a radiation patch and an embedded second-order bandstop filter. Using the same substrate area as a fundamental UWB antenna, a bandstop filter composed of a non-uniform short-circuited stub and coupled open-/short-circuited stub resonators, is designed into the fundamental antenna. A detail design procedure for the proposed antenna with a second-order Maxially-flat bandstop filter at 5.5 GHz is presented. As compared to the fundamental antenna, the proposed UWB antenna provides good notch-band suppression from 5.15 GHz to 5.95 GHz. Also, the proposed structure provides high band-edge selectivity and flat return loss in the notch-band.

***Index Terms*—Band-edge selectivity, filtering antenna, coupled line resonator, stub resonator, total radiated power, ultrawideband antenna.**

Chapter 1 Introduction

With the rapid development of wireless communication systems, the requirements for compact, low-cost, and low profile passive components are demanded in recent years. To achieve these purposes, various efforts could be done in a single circuit module. Integration of antenna and bandpass filter (BPF) in one module is one of the ways to achieve miniaturization and improved performance of microwave front ends. However, to date, there has been relatively little research conducted on an efficient integration between the filter and antenna with simple fabrication and good circuit behavior. Hence, this dissertation mainly focuses on the designs of the compact filtering antennas with good frequency responses by using an efficient co-design method. This chapter firstly describes the motivation of the research, and then briefly reviews surveyed literature. The contributions of this dissertation are presented next. The last section of this chapter is to provide an outline of the following chapters.

Since the size reduction and low profile structure are a trend in the circuit design of a wireless communication systems, it is desired to integrate the bandpass filter and antenna in a single module, so called filtering antenna, with filtering and radiating functions simultaneously. In traditional design, the filter and the antenna are designed individually, with the common ports' characteristic impedance Z_0, and then connected directly. The direct connection of the filter and antenna usually causes an impedance mismatch, which may deteriorate the filter's performance (especially near the band edges) and increase the insertion loss of the circuitry. To avoid this, extra matching network should be implemented in between these two components [1].

Several investigations have been focused on adding the radiating or filtering function into an antenna or filter [2]-[4]. In [2], metal posts were inserted into a horn antenna, which can generate the filtering function. And in [3], the way is to create coupled cavities into a leaky wave antenna so as to generate filtering performance on the antenna. Frequency selectivity surface using cascading substrate integrated waveguide cavity had been designed and directly installed at the aperture of horn antenna [4]. While these proposed circuits possess the characteristics of filtering and radiating, it should be noted that they were designed without using a systematic approach nor considering much on the filter's or antenna's specifications.

Various approaches for integrating the filter and antenna into a single microwave device have been discussed in [5]-[10]. For size reduction, a pre-designed bandpass filter with suitable configuration was directly inserted into the feed position of a patch antenna [5] and a horn antenna [6]. By using an extra impedance transformation structure in between the filter and the antenna, the bandpass filter can be integrated properly with the antenna over the required bandwidth [7]-[9]. However, the transition structure needs additional circuit area, and the designs did not have good filter characteristics over the frequency range. In [10], a mutual synthesis approach was proposed, which considered the conjugate impedance matching in between the filter and antenna. It seems that the matching was performed only at the center frequency, without considering the effect of the antenna's bandwidth and quality factor. Therefore, the main subject of this dissertation is to develop new filtering antennas without using any extra matching circuits or transitions via the co-design method. For the purpose of size reduction and good filter response, several compact structures are presented and established in this research.

In recent years, the popular research studies have appeared that tackle the issue of circuit integration in radio-frequency (RF) front-end of a communication system, such as the integration of filter and antenna. Several filtering antennas designed following the synthesis process of the bandpass filter have been presented [11]-[14]. In these designs, the last resonator and the load impedance of the bandpass filter were substituted by an antenna that exhibited a series or parallel RLC equivalent circuit, as shown in Figure 1.1. Although they have been done based on the co-design approach, most of them did not show good filter performance, especially the band-edge selectivity and stopband suppression. This is due to the lack of the extraction of the antenna's equivalent circuit over a suitable bandwidth. Only that at the center frequency was extracted and used in the filter synthesis. Moreover, the antenna gain versus frequency, which is an important characteristic of the filtering antenna, was not examined in these studies. Although in [14], the frequency response of a factor named *ideal matching loss* (= $1-|S_{11}|^2$) was considered, it did not take into account the circuit and antenna losses and thus missed the power transmission characteristic of the filtering antenna.

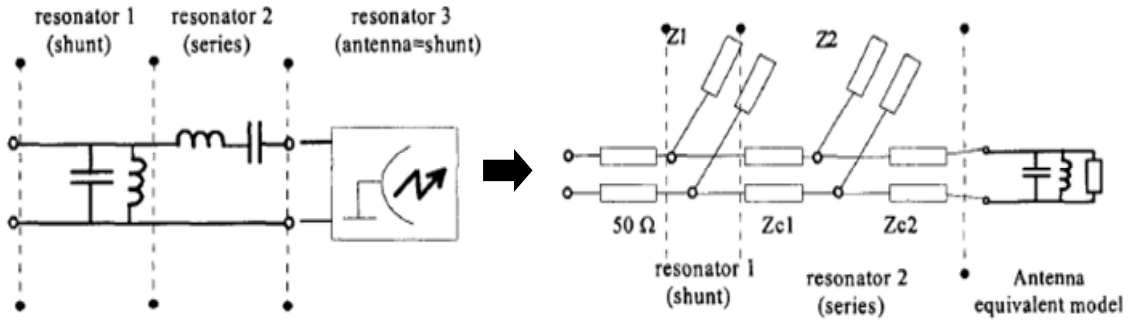

Figure 1.1 Integration of the antenna in the filter structure.

The complicated electromagnetic environment gives a high requirement to the electronic equipments nowadays. Since there are various transmitters and receivers working simultaneously, it is likely to have various interferences. It is noted that the intermodulation (IM) interference is a very serious problem in a communication receiver, because they represent spurious signals and can be mistaken for desired signals. In order to select the interested signal from the promiscuous signal group, the radio receiver system, besides the low noise performance, mainly has the good frequency selectivity. Therefore, the integration of antenna and filter need to meet extensively demanding requirement so that good band-edge selectivity can be achieved.

Generally, filters having transmission zeros at finite frequencies have improved selectivity by using many approaches [15]-[17]. Open-ended resonators with tapped feed [15] and stub-tapped resonators [16] are two good choices to generate transmission zeros on both sides of the passband. A single-triangular open-loop resonator [17], which generates two tunable transmission zeros, possesses a sharp passband skirt and a wide upper stopband up to four times the passband frequency. Cross-coupled filters are also attractive since they exhibit highly selective responses [18]-[21]. A cross-coupled bandpass filter using quarter-wave stepped-impedance resonators (SIRs) on a single circuit plane [18], can produce transmission zeros on both sides of the passband due to the non-adjacent couplings and tapped input/output. The cascade trisection and cascade quadruplet [20], [21] are also two of the most commonly used coupling schemes. The input/output coupling are also well documented to produce transmission zeros. [22], [23]. However, it appears that no research findings are yet available concerning the design of transmission zeros in the integration of a filtering

antenna.

Since the Federal Communications Commission (FCC) has released the bandwidth 3.1–10.6 GHz [24], ultra-wideband (UWB) communication systems attract great attention in the wireless world due to their advantages, including high speed data rate, low power consumption, high capacity, low cost, and low complexity. These UWB systems for communications are especially applied to home networking systems as a technology of wireless personal area networks. As a key component of UWB communication systems, UWB antennas with the fascinated features, such as wide bandwidth, simple structure, and omni-directional radiation pattern, have been widely investigated.

Among the planar UWB antenna designs in the recent literature, the slot and monopole antenna are mainly focused. The advantages of slot antennas include wide bandwidth performance and low cost in the printed circuit board (PCB) process [25]-[27]. The wideband slot antennas can be realized by utilizing a unique tapered-slot feeding structure [25] or a feeding scheme to generate multiple resonances of close bands [26], [27]. Planar monopole antennas have been found as good candidates for UWB applications owing to their attractive merits, such as ultrawide impedance bandwidth, simple structure and ease of fabrication, and good radiation properties. Typical shapes of these antennas are half-disc [28], circle, ellipse [29], [30], rectangle [31], [32], and Binomial curved [33].

In practice, interference is a serious problem for UWB application systems. Despite the approval of the FCC for UWB to operate over 3.1 to 10.6 GHz, it may be necessary to notch-out portions of the band in order to avoid interference with the existing wireless networking technologies such as IEEE 802.11a in the U.S. (5.15–5.35 GHz, 5.725–5.825 GHz) and HIPERLAN/2 in Europe (5.15–5.35 GHz, 5.47–5.725 GHz). This is due to the fact that UWB transmitters should not cause any electromagnetic interference to nearby communication system such as the wireless local area network (WLAN) applications, and vice versa. Therefore, UWB antennas with notched characteristics in the WLAN frequency band are required. There are various methods to achieve the band-notched function. The conventional methods are cutting a slot on the patch [34]-[36], inserting a slit on the patch [37]-[39], or embedding a quarter-wavelength tuning stub within a large slot on the patch [40]. Recently, the band-notched UWB antenna are realized by embedding a pair of T-shaped stubs inside an ellipse slot cut in the radiation patch [41] or using an open-looped resonator at the center of a fork-shaped antenna [42]. Even though these approaches may have good rejection performance, the achieved notch bandwidth is usually limited since only one radiation null is designed in most of these researches. Also, the required transition bandwidth between the pass and notch bands are extended, which will thus encroach upon the usable pass band.

Chapter 2 Coupled Line/Stub Resonators

In this chapter, the novel coupled line and coupled stub resonators are proposed. Section 3.1 illustrates the equivalent circuits and performances of the coupled line resonator, which can provide one pair of transmission zeros with tunable frequencies to achieve the purpose of the high band-edge selectivity. Section 3.1 shows the design of the coupled open-/short-circuited stub resonator with higher equivalent inductance near the center frequency. The proposed structure exhibits a transmission zero at the center frequency and a pair of tunable transmission poles at the two sides.

2.1 Coupled Line Resonator

In the design of a narrow-band bandpass filter, one needs to use shunt *LC* resonators with high capacitances. Although these high-capacitance *LC* resonators can be implemented by using λ/4 short-circuited microstrip stubs, it needs quite large circuit area because of the very wide microstrip line used. In [43, 44], the dual-behavior resonators are designed by associating two different parallel open-circuited stubs. Each stub brings its own transmission zero depending on its fundamental resonant condition. Even so, these resonators also suffer from large circuit area because of the use of the two open-circuited stubs. Recently, the authors proposed the coupled line resonators as shown in Figure (a) [45] to solve this problem, which provides high equivalent capacitance while occupies a reasonable circuit area. In addition, without using the technique of cross-coupling between non-adjacent resonators [46], the proposed coupled line resonator itself produces one pair of tunable symmetric transmission zeros at the two sides of the passband, which greatly increase the band-edge selectivity. In this study, detail analyses of the coupled line resonator are presented. Also, an extended version with different lengths of the coupled lines as shown in Figure (b) is introduced. As will be shown later, this new structure has the advantage of producing two asymmetric transmission zeros that may be contributive to the design flexibility.

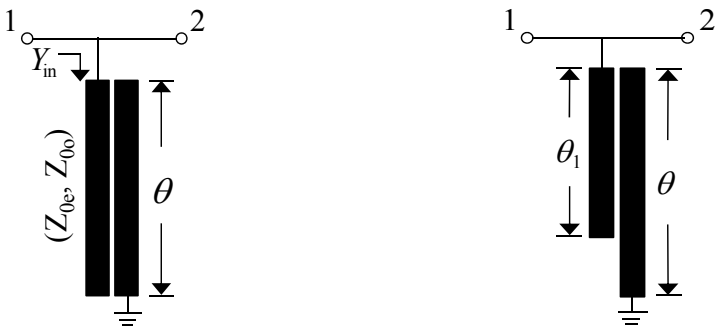

(a) (b)

Figure 2.1 Geometry of the coupled line resonators with (a) equal lengths and (b) unequal lengths.

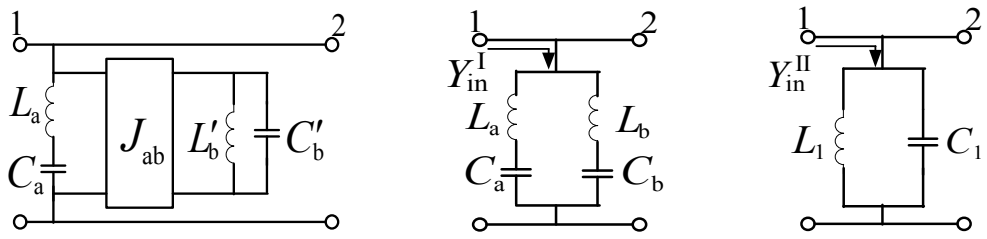

(a) (b) (c)

Figure 2.2 (a) Equivalent circuit of the coupled line resonator with equal lengths. (b) The composite shunt resonator with two series *LC* resonators in parallel. (c) The equivalent shunt *LC* resonator around the resonant frequency f_r.

The coupled line resonator with equal lengths shown in Figure (a) is composed of a quarter-wavelength open-circuited stub and a quarter-wavelength short-circuited stub. These two resonant microstrip stubs couple with each other through the gap between them. Physically, the open-circuited stub is equivalent to a series *LC* resonator, and the short-circuited stub a shunt *LC* resonator. And the coupling gap, which mainly offers electrical coupling between the resonators, functions as an admittance inverter (or *J*-inverter) [47]. Therefore, the proposed structure can be equivalent to the circuit shown in Figure (a). Note that due to the presence of the coupling, the two resonators (L_a, C_a) and (L'_b, C'_b) have different resonant frequencies, although the two coupled stubs are with equal lengths. This equivalent circuit can be further transformed into the circuit shown in Figure (b), which consists of two series *LC* resonators connected in parallel, with resonant frequencies at f_a and f_b, respectively. It is thus evident that the proposed structure provides two transmission zeros at these two resonant frequencies.

We now set up the quantitative equivalence between the coupled line resonator (Figure (a)) and the equivalent circuit (Figure (b)) in the following three steps: First, derive the input admittances of the circuits; secondly, equate the two admittances and their derivatives, respectively, at the center frequency, and also let the two circuits with the same transmission zeros; thirdly, extract the equivalent circuit components from the above-obtained equations.

In the first step, one first derives the admittances of these two circuits as [47]:

$$Y_{in} = -j\frac{(Z_{0e}+Z_{0o})\sin 2\theta}{(Z_{0e}-Z_{0o})^2-(Z_{0e}+Z_{0o})^2\cos^2\theta} \tag{2.1a}$$

$$Y_{in}^{I} = -j\left[\frac{1}{2\pi f L_a\left(1-\frac{f_a^2}{f^2}\right)}+\frac{1}{2\pi f L_b\left(1-\frac{f_b^2}{f^2}\right)}\right] \tag{2.1b}$$

where Y_{in} and Y_{in}^{I} are the admittances of the coupled line resonator and the equivalent circuit in Figure (b), respectively. Z_{0e} and Z_{0o} are the even-mode and odd-mode impedances of the coupled line. θ is the

electrical length, $\theta = \frac{\pi f}{2 f_r}$, with f_r the corresponding resonant frequency. $f_a = \left(2\pi\sqrt{L_a C_a}\right)^{-1}$, $f_b = \left(2\pi\sqrt{L_b C_b}\right)^{-1}$. Note that, like the equivalent *LC* circuit, the coupled line resonator has a transmission pole ($Y_{in} = 0$) at $\theta = \pi/2$ (or $f = f_r$) and two transmission zeros ($Y_{in} \to \infty$) at $\theta = \sin^{-1}\left(\frac{2\sqrt{Z_{0e}Z_{0o}}}{Z_{0e}+Z_{0o}}\right)$ and $\pi - \sin^{-1}\left(\frac{2\sqrt{Z_{0e}Z_{0o}}}{Z_{0e}+Z_{0o}}\right)$. It is noticed that the two zeros are symmetric to the transmission pole.

In the second step, the circuit shown in Figure (b) is equivalent to the coupled line resonator by letting $Y_{in}(f_r) = Y_{in}^{I}(f_r)$, $\left.\frac{dY_{in}}{df}\right|_{f_r} = \left.\frac{dY_{in}^{I}}{df}\right|_{f_r}$, and also making their transmission zeros the same. One then obtains the following four equations:

$$\frac{1}{2\pi f_r L_a\left(1-\frac{f_a^2}{f_r^2}\right)} + \frac{1}{2\pi f_r L_b\left(1-\frac{f_b^2}{f_r^2}\right)} = 0 \tag{2.2a}$$

$$\frac{1+\frac{f_a^2}{f_r^2}}{2\pi f_r L_a\left(1-\frac{f_a^2}{f_r^2}\right)^2} + \frac{1+\frac{f_b^2}{f_r^2}}{2\pi f_r L_b\left(1-\frac{f_b^2}{f_r^2}\right)^2} = \pi\frac{Z_{0e}+Z_{0o}}{(Z_{0e}-Z_{0o})^2} \tag{2.2b}$$

$$f_a = \frac{2f_r}{\pi}\sin^{-1}\left(\frac{2\sqrt{Z_{0e}Z_{0o}}}{Z_{0e}+Z_{0o}}\right) \tag{2.2c}$$

$$f_b = 2f_r - f_a \tag{2.2d}$$

Once the dimensions of the coupled line resonator are given, f_r, Z_{0e}, and Z_{0o} will be determined. In the last step, one can thus get the four circuit parameters (L_a, C_a, L_b, C_b) in Figure (b) by solving these four equations.

Furthermore, near the resonant frequency f_r, the coupled line resonator can be approximated as a shunt *LC* resonator, as shown in Figure (c), since one of the series *LC* resonators in Figure (b) shows inductive property and the other capacitive at the frequency in between f_a and f_b. The equivalence between these two circuits are established by equalizing their resonant frequencies and the admittance derivatives, which yield

$$f_r = \frac{1}{2\pi\sqrt{L_1 C_1}} \tag{2.3}$$

and

$$\frac{(Z_{0e}+Z_{0o})}{(Z_{0e}-Z_{0o})^2}=\frac{2}{\pi}\sqrt{\frac{C_1}{L_1}} \tag{2.4}$$

The circuit components L_1, C_1 can thus be calculated while the impedances (Z_{0e}, Z_{0o}) and f_r are given.

Figure shows the circuit simulation results by AWR [48] for a coupled line resonator with line width of 0.5 mm and gap 0.2 mm, fabricated on a 0.508 mm thick Rogers 4003 substrate with a dielectric constant 3.38 and loss tangent of 0.0027. Here, the ideal transmission lines for the coupled line resonator are considered. The electric length of the coupled lines is $\theta = 90°$, which corresponds to a resonant frequency at 2.5 GHz. To get the equivalent circuits, one first calculates the impedances Z_{0e} and Z_{0o} as 100 Ω and 57 Ω, respectively. Then, based on (2.2c) and (2.2d), the two transmission zeros, f_a and f_b, are calculated to be 2.05 GHz and 2.95 GHz. Finally, the circuit components in Figure (b) and (c) can be obtained by using (2.2a), (2.2b), (2.3), and (2.4), which are (L_a, C_a) = (8.46 nH, 0.71 pF), (L_b, C_b) = (7.07 nH, 0.41 pF), and (L_1, C_1) = (0.49 nH, 8.26 pF). It is seen from the figure that, the frequency responses of the equivalent circuit in Figure (b) match very well with those of the coupled line resonator over the full frequency band. Not only with the same transmission pole and zeros, the curves are completely overlapped in the frequency range between f_a and f_b. Also, the responses of the circuit in Figure (c) agree well with the ones of the coupled line resonator near the resonant frequency f_r.

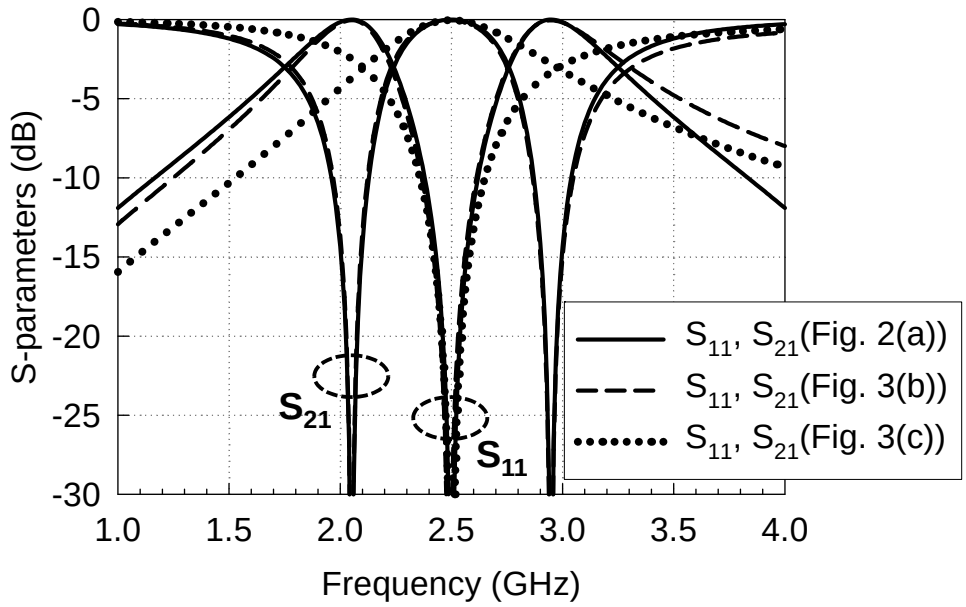

Figure 2.3 Circuit simulation of the coupled line resonator with equal lengths in comparison with the ones of its corresponding equivalent circuits (Figs. 3.2(b) and (c)). The line width and gap size of the coupled line resonator are 0.5 mm and 0.2 mm.

As will be shown later, when designing a filtering antenna, the equivalent circuit components are first obtained based on the filter specifications, from which the structure dimensions have to be decided. To this end, one may use (2.2c) and (2.4) to derive the even- and odd-mode characteristic impedances of the coupled line resonator as:

$$Z_{0e}=\frac{1}{2k_2}\left[\frac{1}{1-k_1}+\frac{1}{\sqrt{1-k_1}}\right] \tag{2.5a}$$

$$Z_{0o} = \frac{1}{2k_2}\left[\frac{1}{1-k_1} - \frac{1}{\sqrt{1-k_1}}\right] \tag{2.5b}$$

where $k_1 = \sin^2\left(\frac{\pi f_a}{2f_r}\right)$, $k_2 = \frac{2}{\pi}\sqrt{\frac{C_1}{L_1}} = 4f_r C_1$.

These impedances together with the given resonant frequency f_r can then be used to determine the resonator's dimensions [47].

In many applications, the required transmission zeros of a bandpass filter are not symmetric to the passband. It is thus necessary to modify the proposed resonator structure shown in Figure (a) that possesses symmetric zeros. One of the solutions is shown in Figure (b), in which the short-circuited stub remains the same length, i.e., $\theta = \pi/2$ at the resonant frequency, while the open-circuited stub has a length longer ($\theta_1 > \pi/2$) or shorter ($\theta_1 < \pi/2$). Figure 2.4 shows the circuit simulation results for the coupled line resonators with different θ_1. The structure parameters are the same as those in Figure except the length of the open-circuited stub. It is observed that, as θ_1 is decreased or increased from $\pi/2$, the resonant frequency remains the same but the two transmission zeros move toward the higher or lower frequencies, as shown in Figure 2.4(a) and (b), respectively. Furthermore, for the reason that a smaller circuit area is usually required and the fact that the higher transmission zero moves much faster than the lower one, the case of shorter θ_1 is chosen in this study. In application, one may first design a coupled line resonator with equal length to determine the resonant frequency f_r and the approximate the frequency of the lower transmission zero, and then adjust the frequency of the higher transmission zero to the desired one by tuning the open stub's length. Note that as depicted in Figure 2.4(a), the characteristics of the coupled line resonator keep the same at frequencies near f_r, which means that, when incorporating this resonator into a bandpass filter, the filter's passband performance will not change due to the adjustment of the higher transmission zero. Another solution, that the open-circuited stub has a length $\theta = \pi/2$ while the short-circuited stub has a variable length can also provide asymmetric transmission zeros but would have different resonant frequency f_r, which is thus not considered here.

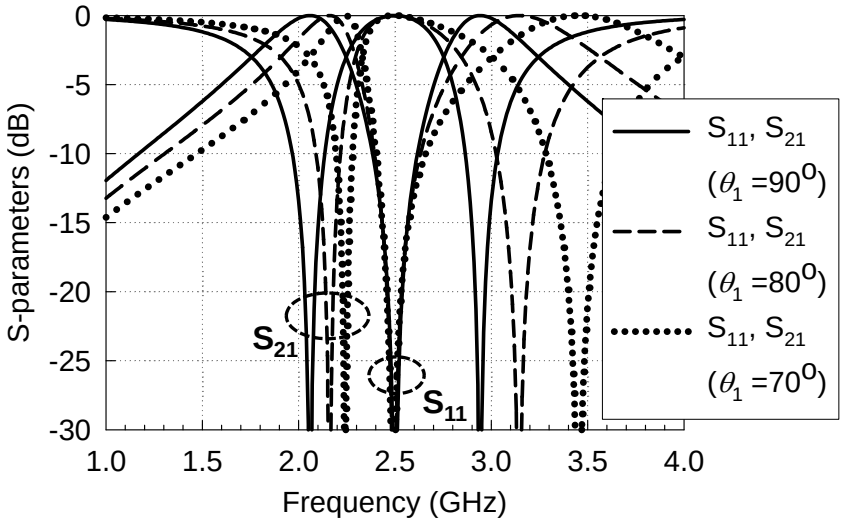

(a)

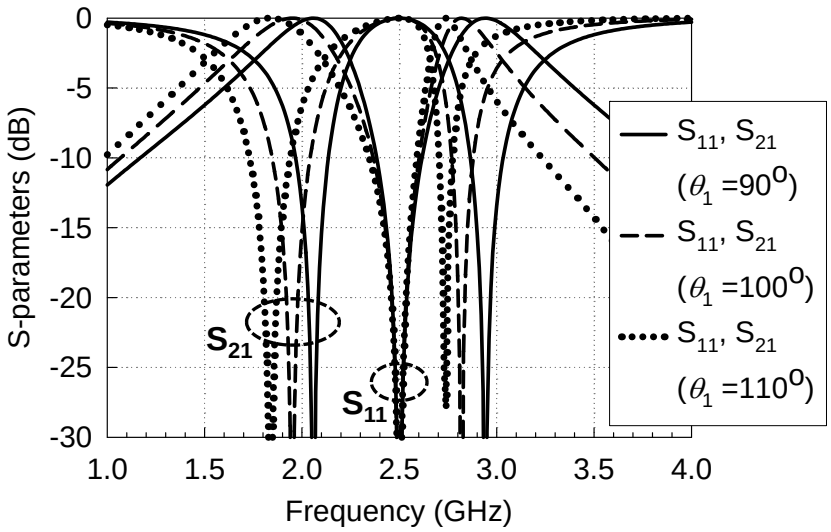

(b)

Figure 2.4 Circuit simulation of the coupled line resonator with unequal lengths for different θ_1. (a) θ_1 decreases from $\pi/2$. (b) θ_1 increases from $\pi/2$.

2.2 Coupled Open-/Short-Circuited Stub Resonator

To realize the series *LC* resonator, one usually uses a λ/4 open-circuited microstrip stub. However, this resonant stub shows only a transmission zero at the resonant frequency, and thus presents low skirt selectivity at the band edges. A λ/4 open-/short-circuited stub resonator [49], as shown in Figure (a), had been proposed to increase the band-edge selectivity. This circuit behaves as a series *LC* resonator at the center frequency due to the λ/4 open-circuited stub. And at a frequency lower (higher) than the center one, the open-circuited (short-circuited) stub shows a capacitive reactance and the short-circuited (open-circuited) stub an inductive reactance, so that the whole circuit behaves as a shunt *LC* resonator. It turns out that the open-/short-circuited stub resonator exhibits a transmission zero at the center frequency and a pair of symmetric transmission poles at the two sides. Nevertheless, due to the low inductance of the series *LC* resonator near the center frequency, this stub resonator presents wider notch-band bandwidth, which is not suitable for designing a narrow-band bandstop filter as that in the present study.

To solve this problem, here we propose a coupled λ/4 open-/short-circuited stub resonator as shown in Figure (b). Moreover, an extended version with different lengths of coupled stubs as shown in Figure (c) is also introduced. As shown below, this new structure exhibits higher inductance near the center frequency due to the introduction of the coupling mechanism, which fits the requirement of the current design. It also has the advantage of producing a pair of asymmetric transmission poles that is contributive to the design flexibility. Besides these good points, the new structure occupies less circuit area due to the close spacing of the two stubs. As the conventional structure, the coupled stub resonator can be equivalent to a series *LC* resonator (Figure (d)) near the center frequency.

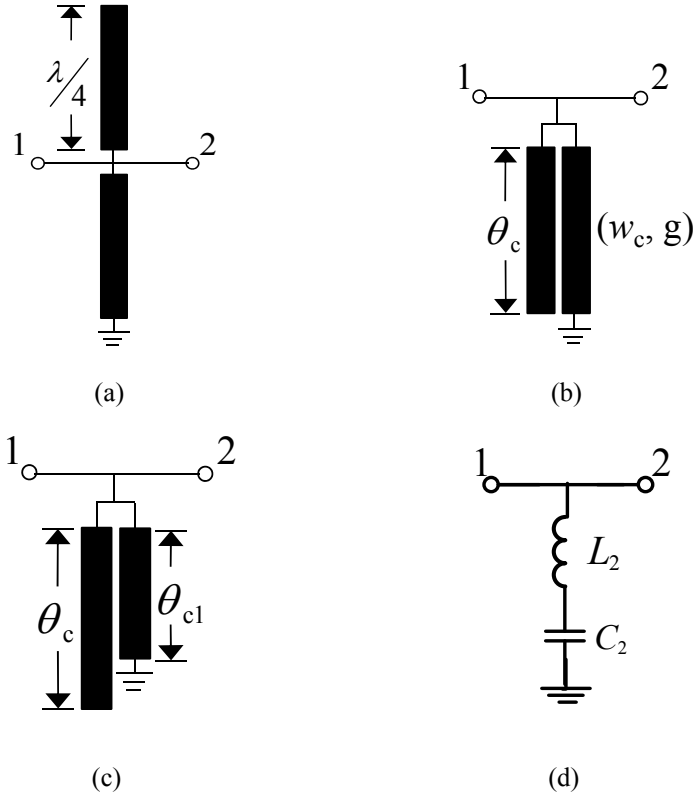

Figure 2.5 The open-/short-circuited stub resonator: (a) conventional type with equal lengths; proposed coupled type (b) with equal lengths and (c) with unequal lengths. (d) The equivalent series *LC* resonator near center frequency of these stub resonators.

Figure shows the extracted equivalent inductance L_2 at the center frequency (f_0= 5.5 GHz) of the coupled open-/short- circuited stub, as a function of the strip width w_c that fabricated on a 0.4mm thick FR4 substrate by using AWR. The result for the conventional structure is also shown for reference. It is obvious that for each strip width, the proposed structure gets more than twice the equivalent inductance of the conventional one. Figure depicts the simulated reflection coefficient (S_{11}) and transmission coefficient (S_{21}) of the coupled stub resonator with different lengths. Here the open-circuited stub has a fixed length $\theta_c = 90°$ (or a quarter wavelength) at 5.5 GHz. The results for different short-circuited stub lengths ($\theta_{c1} = 90°$, 80°, 70°) are shown for comparison. It is first observed that the response near the center frequency (5.5 GHz) is unchanged as the stub length θ_{c1} decreases from 90° to 70°. This means that the corresponding equivalent circuit (the series *LC* resonator) is not influenced by θ_{c1}. The structure possesses two transmission poles symmetrically located at 3.3 GHz and 7.5 GHz when the two stubs are with equal length ($\theta_{c1} = \theta_c = 90°$). As the length of short-circuited stub decreases, both the transmission poles move to higher frequencies while the transmission zero remains at 5.5 GHz. The frequency shifts for the two transmission poles are different. The higher transmission pole moves faster than the lower one. For designing a bandstop filter, the controlling of transmission poles' locations are important since they will influence the filter's out-band (passband) bandwidth and performance. The proposed coupled stub resonator not only possesses high inductance near the center frequency but also provides an extra degree of freedom in controlling the passband characteristics.

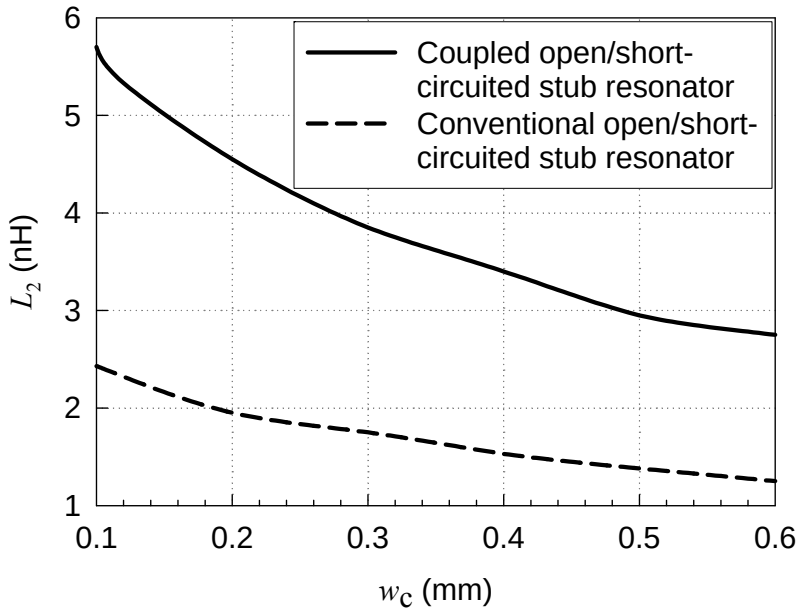

Figure 2.6 The inductance L_2 of the coupled open-/short-circuited stub resonator as a function of the strip width w_c in comparison with the one of the conventional structure. (g = 0.12 mm and $\theta_{c1} = \theta_c = 90°$ at f = 5.5 GHz)

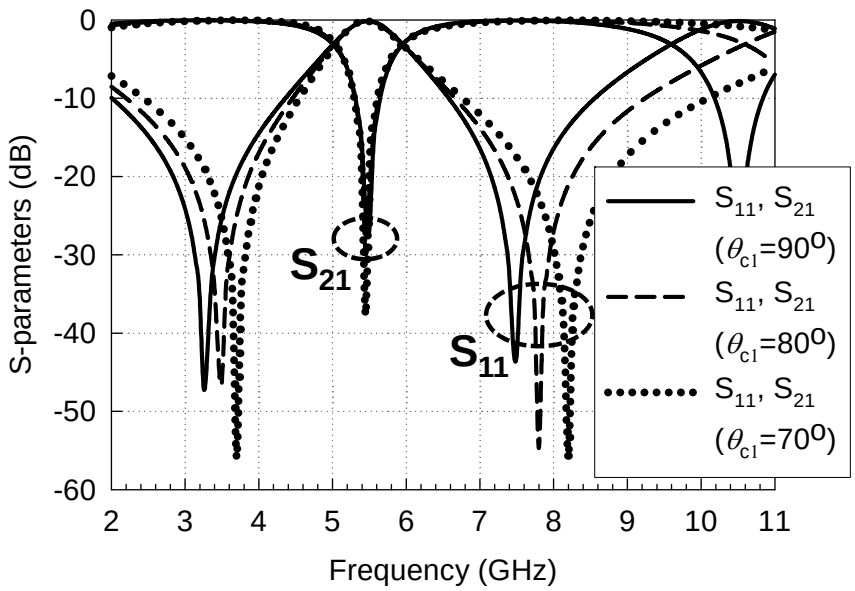

Figure 2.7 Circuit simulation of the coupled open-/short-circuited stub resonator with unequal lengths for different θ_{c1}. (w_c = 0.5 mm)

Chapter 3 Compact Filtering Antennas

In this chapter, three types of compact filtering antennas have been proposed. For the requirements of efficient integration and simple fabrication, the new co-design approach for the integration of filter and antenna is introduced. The equivalent circuit models for the inverted-L and inverted-F antenna (ILA and IFA), which are mainly a series RLC circuit, are first established. The values of the corresponding circuit components are then extracted by comparing with the full-wave simulation results. The antennas here perform not only a radiator but also the last resonator of the bandpass filter. A new filtering antenna with printed structure, which contains an inverted-L antenna and the parallel coupled microstrip line resonator, are first presented to illustrate the synthesis of a bandpass filtering antenna. Moreover, the novel compact printed filtering antennas, which are composed of a miniaturized coupled line resonator and different type antenna, are proposed.

3.1 Equivalent Circuit Model of Antennas

Since the antenna is to be designed in the filter as the last resonator, the first step to synthesize the filtering antenna is to establish the antenna's equivalent circuit model and extract the circuit components. In this research, the printed inverted-L antenna and inverted-F antenna are used with its equivalent circuits completely extracted over a desired bandwidth for the synthesis of the filtering antennas.

3.1.1 Inverted-L Antenna

Figure (a) and (b) show the dimensions of the inverted-L antenna and the corresponding equivalent circuit at the antenna feed point looking toward the antenna. Since the inverted-L antenna is a variety of a monopole antenna, the antenna exhibits a series RLC resonance near the first resonant frequency [50]. Here, L_A and C_A express the resonant inductance and capacitance of the antenna, respectively, and R_A corresponds to the antenna radiation resistance. It is noted that an extra shunt capacitance C_g is incorporated in the equivalent circuit here so that, as will be seen below, the whole circuit would have the same impedance behavior as the antenna itself in a wider frequency range. This parasitic capacitance comes from the accumulation of charges around the antenna feed point due to the truncation of the ground plane.

The inverted-L antenna is printed on a 0.508 mm Rogers 4003 substrate with a dielectric constant of 3.38 and loss tangent of 0.0027. The ground plane of the antenna, which is also the ground plane of the circuitry, has a fixed size of $L \times W = 60$ mm $\times$ 60 mm. The antenna is fed through a 50 Ω microstrip line of width 1.17 mm. In the following, the simulated characteristics of all the structures (filters and antennas) are performed by the full-wave simulator Ansoft HFSS (High Frequency Structure Simulator based on the finite element method) [51], while those of the antenna's equivalent circuit are by AWR MWO (Microwave Office) [48]. For each given inverted-L antenna structure, the equivalent circuit components are extracted by first letting the resonant frequency of the circuit equal the simulated resonant frequency of the antenna. And then,

we optimize the values of the circuit components so that the reflection coefficient (S_{11}), as a function of frequency, of the equivalent circuit coincides with that simulated from the antenna in a frequency range as wide as possible. The difference ΔS_{11} of the reflection coefficient between these two curves is set not beyond 3% in a 20% frequency bandwidth centered at the antenna resonant frequency.

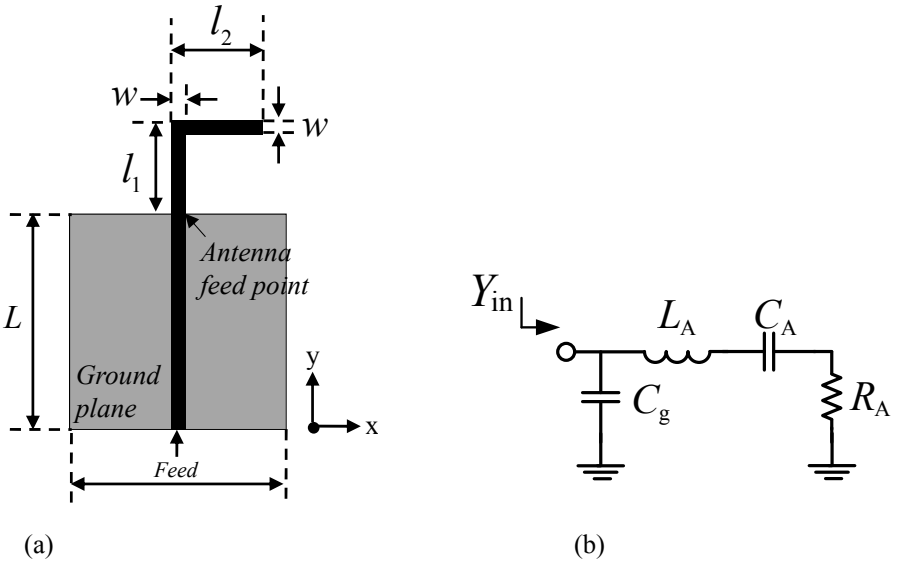

(a) (b)

Figure 3.1 (a) Configuration of the inverted-L antenna. (b) The corresponding equivalent circuit of the inverted-L antenna.

In this design, the radiation resistance R_A in the equivalent circuit can serve as the load impedance of the bandpass filter to be synthesized, and the series L_A-C_A circuit can be the filter's last resonator so that

$$f_0 = \frac{1}{2\pi\sqrt{L_A C_A}} \tag{3.1}$$

where f_0 is the center frequency of the bandpass filter and is chosen as 2.45 GHz in this work. In the process of establishing the antenna database, the antenna frequency f_A, which is determined by the total strip lengths ($l_1 + l_2 \approx \lambda_A/4$), should be slightly larger than f_0 due to the existence of the parasitic capacitance C_g. This frequency corresponds to the frequency location of the minimum value of the antenna's reflection coefficient (S_{11}):

$$S_{11} = 20\log\left|\frac{Y_{in} - Y_0}{Y_{in} + Y_0}\right| \tag{3.2a}$$

with

$$Y_{in} = j2\pi f C_g + \left[R_A + j2\pi f L_A (1 - \frac{f_0^2}{f^2}) \right]^{-1} \tag{3.2b}$$

It is noted that the radiation resistance R_A and the inductance L_A are mainly dependent on the vertical strip length l_1 due to the strongest current distribution on this strip. Also, the parasitic capacitance C_g is decided by the strip width w and independent of the strip length l_1. It is thus observed that the values of the

three components (R_A, L_A, C_g) in (3.2) are almost invariant at a fixed strip length l_1 only if the antenna frequency is near f_0. Therefore, for a choosing strip length, we first extract the components of the R_A, L_A, and C_g when the antenna is resonated at f_0, and then, taking these three components into (3.2), the resonant frequency f_A can be obtained. Various values of l_1 have been analyzed in this study. It is found out that, the antenna with different dimensions of l_1 has the resonant frequency f_A near 2.53 GHz while f_0 is 2.45GHz.

Another important factor to be used for synthesizing the filtering antenna is the corresponding quality factor of the antenna, Q_A, which is defined as

$$Q_A = \frac{2\pi f_0 L_A}{R_A} \tag{3.3}$$

and is that of the series RLC circuit in the antenna's equivalent circuit, without including the effect of the parasitic capacitance C_g. It should be noticed that the Q_A is not the whole quality factor of the inverted-L antenna.

Figure shows the variation of the radiation resistance R_A and quality factor Q_A as a function of the vertical strip length l_1. It can be observed that the radiation resistance R_A increases substantially from 13.6 Ω to 36.8 Ω when the strip length l_1 changes from 5 mm to 13 mm. In the same l_1 variation range, the inductance L_A (not shown in this figure) has only little change (from 12 nH to 14.5 nH). The radiation resistance increases much fast than the inductance as the strip length increases, which results in a decreasing quality factor due to (3.3). As seen, the quality factor changes from 13.7 to 6.0 when l_1 increases from 5 mm to 13 mm. Although not shown here, the strip width w has minor influence on the values of equivalent circuit components. And the extracted parasitic capacitance C_g is around 0.3 pF to 0.4 pF, roughly independent of the variations of l_1 and w. As to the application in the synthesis of the proposed filtering antenna, once the quality factor Q_A is determined by the given specifications of filter (the relationship will be derived later), the values of l_1 and R_A can be obtained via the Q_A-to-l_1 and R_A-to-l_1 curves in Figure , respectively, and then the dimensions of the antenna can be obtained.

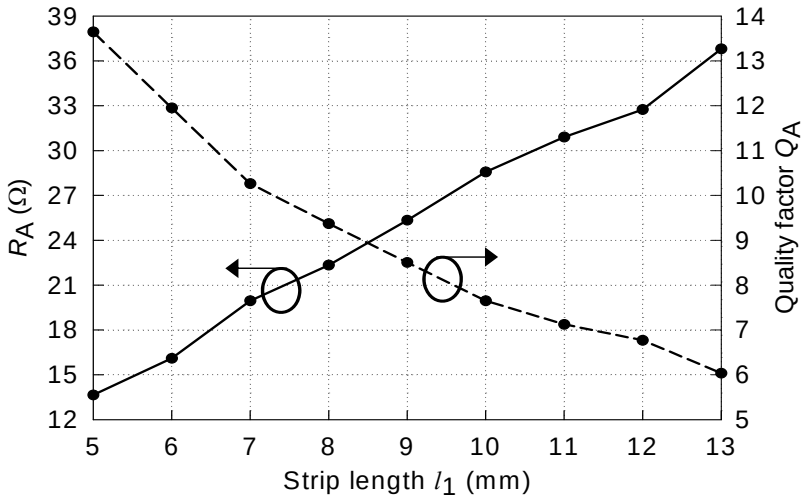

Figure 3.2 The radiation resistance R_A and quality Q_A as a function of the strip length l_1. w = 1.17 mm, f_0 = 2.45 GHz.

Figure shows the comparison of the impedance behaviors on the Smith chart from the full-wave simulation and the equivalent circuit calculation. The dimensions of the inverted-L antenna, which is to be used later in the synthesis of the filtering antenna, are l_1 = 10 mm, w = 1.17 mm, and l_2 = 17.25 mm. The extracted circuit components are L_A = 14.2 nH, C_A = 0.30 pF, R_A = 28.6 Ω, and C_g = 0.37 pF, with the corresponding quality factor Q_A = 7.65. Notice that C_g has the same level as C_A so that this parasitic capacitance can not be neglected in the modeling of the antenna. It is seen from the figure that the curve of S_{11} for the equivalent circuit agrees well with the full-wave simulation one from 1.5 GHz to 4 GHz. Especially, they have the same value at the antenna resonant frequency (f_A = 2.53 GHz), and the difference ΔS_{11} is 0.16 dB (error of $S_{11} \approx 3\%$) at f = 2.28 GHz and 0.148 dB (error of $\Delta S_{11} \approx 3\%$) at f = 2.81 GHz.

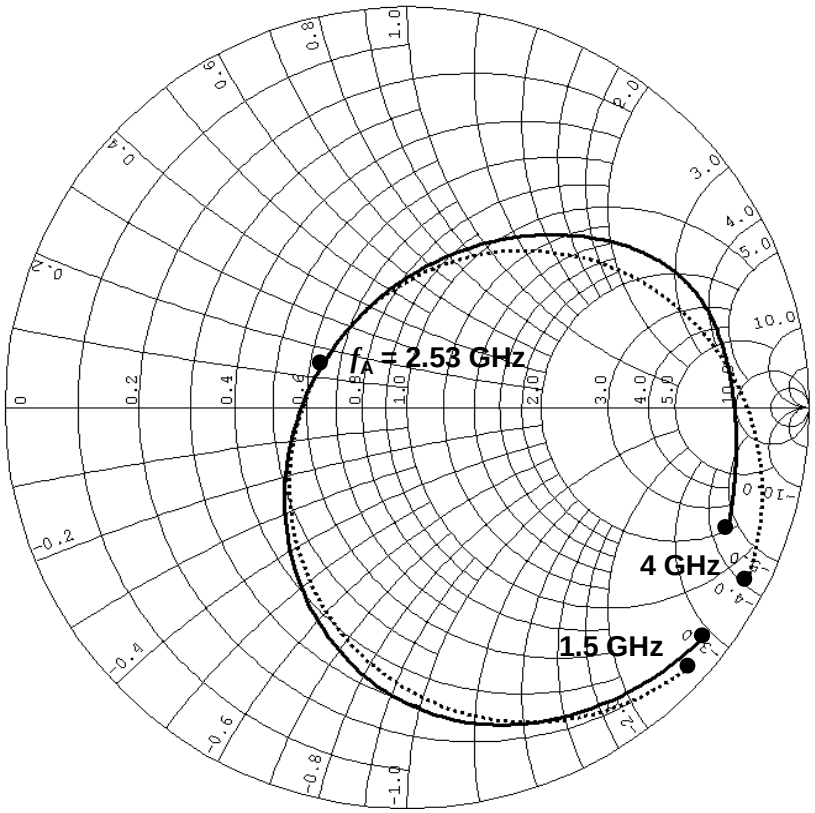

Figure 3.3 Input impedances of the inverted-L antenna with l_1 = 10 mm, w = 1.17 mm, and l_2 = 17.25 mm. (solid line: the full-wave simulation; dotted line: the equivalent circuit calculation.

3.1.2 Inverted-F Antenna

Figure 3.4(a) and (b) shows the dimensions of the inverted-F antenna and the corresponding equivalent circuit at the antenna feed point looking toward the antenna. The inverted-F antenna can be modeled as a short-circuited transmission line of length θ_s in shunt with a main series RLC resonance near the first resonant frequency [52]. Here, L_A and C_A express the resonant inductance and capacitance of the antenna, respectively. R_A is the antenna radiation resistance produced by the vertical strips, including the left- and right-side strips in Figure 3.4(a). Alternately, the inverted-F antenna is treated as a small loop inductor, which can be seen a short-circuited transmission line, consisting of the two vertical strips and horizontal strip l_2.

The inverted-F antenna is printed on a 0.8 mm RF4 substrate with a dielectric constant of 4.4 and loss

tangent of 0.02. The ground plane of the antenna, which is also the ground plane of the circuitry, has a fixed size of $L \times W = 50$ mm $\times$ 50 mm. The antenna is fed through a 50 Ω microstrip line of width 1.53 mm. Using the same approach of extraction in Section 3.1.1, the equivalent circuit components for the different sizes of the inverted-F antenna can be extracted by first letting the resonant frequency of the circuit equal the simulated resonant frequency of the antenna. And then, we optimize the values of the circuit components so that the reflection coefficient (S_{11}), as a function of frequency, of the equivalent circuit coincides with that simulated from the antenna in a frequency range as wide as possible. The difference ΔS_{11} of the reflection coefficient between these two curves is set not beyond 3% in a 20% frequency bandwidth centered at the antenna resonant frequency.

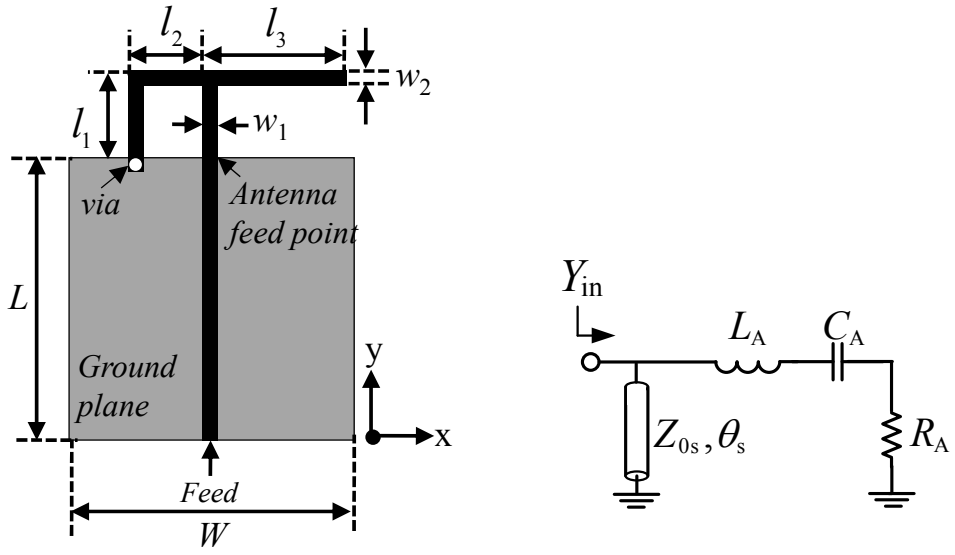

Figure 3.4 (a) Configuration of the inverted-F antenna. (b) The corresponding equivalent circuit of the inverted-F antenna.

Note that the radiation resistance R_A in the equivalent circuit of the inverted-F antenna can serve as the load impedance of the bandpass filter to be synthesized, and the series L_A-C_A circuit in Figure 3.4(b) can be the filter's last resonator has the \relation as (3.4). In the process of establishing the antenna database, the antenna frequency f_A, which is determined by the total strip lengths ($l_1 + l_2 + l_3 \approx \lambda_A/4$), should be slightly smaller than f_0 due to the existence of the short-circuited transmission line. It is found out that the antenna frequency f_A is near 2.43 GHz ($f_0 = 2.45$ GHz) while l_1 is short. When l_1 is increased, the f_A is almost close to f_0 due to higher inductive reactance of the short-circuited transmission line are appeared. The frequency corresponds to the frequency location of the minimum value of the antenna's reflection coefficient (S_{11}) can be calculated by using (3.2a), where

$$Y_{in} = -jY_{0s}\cot\theta_s + \left[R_A + j2\pi f L_A\left(1 - \frac{f_0^2}{f^2}\right)\right]^{-1} \tag{3.4}$$

It is noted that the radiation resistance R_A and the inductance L_A are mainly dependent on these two vertical strips length l_1 due to the strongest current distribution on this strip. It is thus observed that the values of the two components (R_A, L_A) and (Z_{0s}, θ_s) in (3.2a) are almost invariant at a fixed strip length l_1 and l_2 only if the antenna frequency is near f_0. Therefore, for a choosing strip length, we first extract the

components of the R_A, L_A, and (Z_{0s}, θ_s) when the antenna is resonated at f_0, and then, taking these three components into (3.2a), the resonant frequency f_A can be obtained. Various values of l_1 have been analyzed in this study. It is found out that, the antenna with different dimensions of l_1 has the resonant frequency f_A between 2.41 GHz to 2.45 GHz while f_0 is 2.45GHz.

Figure 3.5(a) shows the variation of the radiation resistance R_A and quality factor Q_A as a function of the vertical strip length l_1 and fixed l_2. It can be observed that the radiation resistance R_A increases substantially from 25 Ω to 95 Ω when the strip length l_1 changes from 5 mm to 13 mm. In the same l_1 variation range, the inductance L_A (not shown in this figure) has only little change (from 12 nH to 14.5 nH). The radiation resistance increases much fast than the inductance as the strip length increases, which results in a decreasing quality factor due to (3.3). As seen, the quality factor changes from 13.7 to 6.0 when l_1 increases from 5 mm to 13 mm. Although not shown here, the strip width w has minor influence on the values of equivalent circuit components. As to the application in the synthesis of the proposed filtering antenna, once the quality factor Q_A is determined by the given specifications of filter (the relationship will be derived later), the values of l_1 and R_A can be obtained via the Q_A-to-l_1 and R_A-to-l_1 curves in Figure 3.4(a), respectively, and then the dimensions of the antenna can be obtained. Figure 3.5(b) shows the variation of the radiation resistance R_A and quality factor Q_A as a function of the vertical strip length l_2 and fixed l_1. It is shown that the radiation resistance R_A and quality factor Q_A only have a little decrease when the strip length l_2 changes from 2 mm to 10 mm.

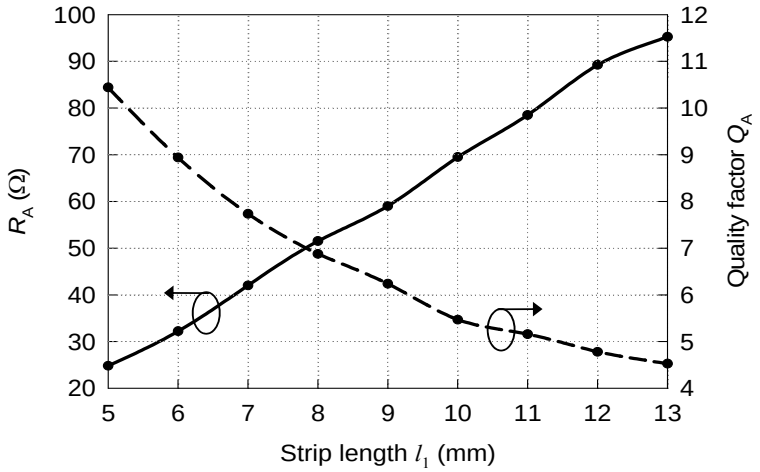

(a)

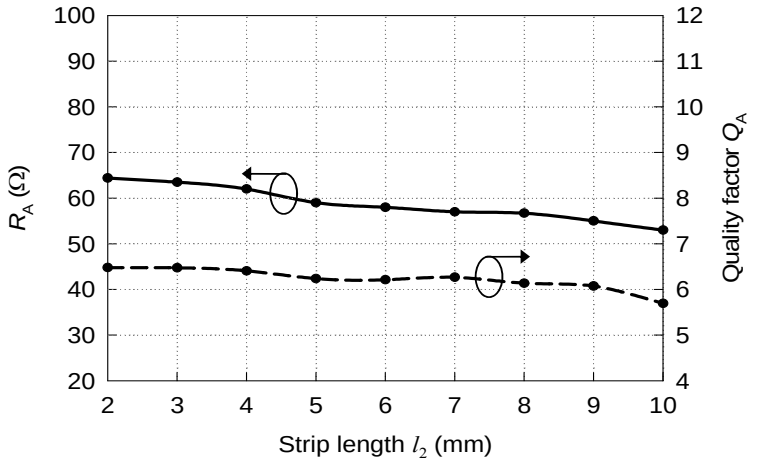

(b)

Figure 3.5 The radiation resistance R_A and quality Q_A as a function of the (a) strip length l_1 and fixed l_2 = 5 mm and (b) strip length.

l_2 and fixed l_1 = 9mm. w_1 = 1.53 mm, w_2 = 1 mm, f_0 = 2.45 GHz.

Figure 3.6 shows the comparison of the impedance behaviors on the Smith chart from the full-wave simulation and the equivalent circuit calculation. The dimensions of the inverted-F antenna are l_1 = 9 mm, l_2 = 5 mm, l_3 = 18 mm, w_1 = 1.53 mm, and w_2 = 1 mm. The extracted circuit components are L_A = 23.9 nH, C_A = 0.177 pF, R_A = 59 Ω, Z_{0s} = 220 Ω, and θ_s = 83°, with the corresponding quality factor Q_A = 6.24 using (3.3). It is seen from the figure that the curve of S_{11} for the equivalent circuit agrees well with the full-wave simulation one from 1.5 GHz to 4 GHz.

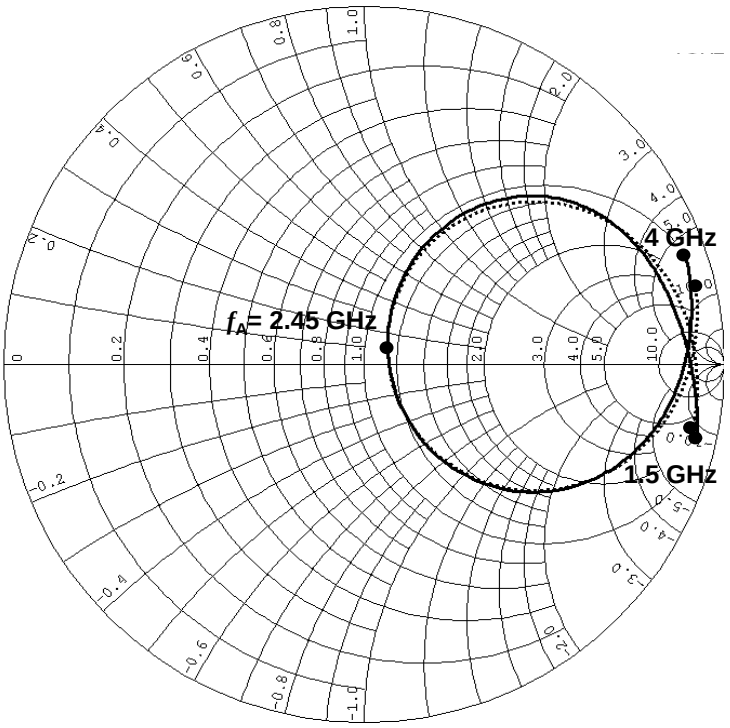

Figure 3.6 Input impedances of the inverted-F antenna with l_1 = 9 mm, l_2 = 5 mm, l_3 = 18 mm, w_1 = 1.53 mm, and w_2 = 1 mm while antenna frequency f_A is close to f_0 = 2.45 GHz. (solid line: the full-wave simulation; dotted line: the equivalent circuit calculation.

3.2 Synthesis and Design of a New Printed Filtering Antenna

Synthesis and design of a new printed filtering antenna is firstly presented in this section, as shown in Figure 3.7. For the requirements of efficient integration and simple fabrication, the co-design approach for the integration of filter and antenna is introduced. The printed inverted-L antenna and the parallel coupled microstrip line sections are used for example to illustrate the synthesis of a bandpass filtering antenna. The inverted-L antenna here performs not only a radiator but also the last resonator of the bandpass filter. A design procedure is given, which clearly indicates the steps from the filter specifications to the implementation. As an example, a 2.45 GHz third-order Chebyshev bandpass filter with 0.1 dB equal-ripple response is tackled. Without suffering more circuit area, the proposed structure provides good design accuracy and filter skirt selectivity as compared to the filter simple cascade with antenna and a bandpass filter of the same order. The measured results, including the return loss, total radiated power, and radiation gain versus frequency, agree well with the designed ones.

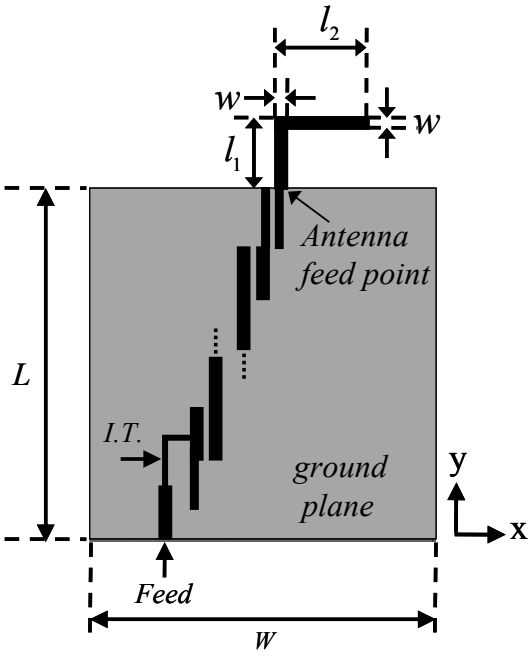

Figure 3.7 Configuration of the proposed filtering antenna.

3.2.1 Synthesis of the Filtering Antenna

Figure 3.8(a) shows the proposed filtering antenna, which contains N coupled line sections and an inverted-L antenna. Note that the antenna is connected directly to the N-th coupled line. The filter to be synthesized is an N-th order Chebyshev bandpass filter. The N-1 filter resonators are provided by the coupled line sections and the last one by the inverted-L antenna. In order to match to the low antenna radiation resistance and increase the flexibility of design, here the N-th coupled line has different design as the conventional ones. Consider a coupled line section with even- and odd-mode characteristic impedances Z'_{0eN} and Z'_{0oN}, respectively, as shown in Figure (a), which is to be equivalent to the circuit shown in Figure (b) near the center frequency f_0. The right transmission line section in Figure (b) has a characteristic impedance Z_a, which is different from the system impedance Z_0 (= 50 Ω) and can be selected arbitrarily. To have the same circuit performances near the center frequency, the ABCD matrices of the coupled line section and the equivalent circuit should be equal at $\theta' = \pi/2$, resulting into

$$Z'_{0eN} = Z_a\left[Z_0/Z_a + J'_N Z_0 + \left(J'_N Z_0\right)^2\right] \tag{3.5a}$$

$$Z'_{0oN} = Z_a\left[Z_0/Z_a - J'_N Z_0 + \left(J'_N Z_0\right)^2\right] \tag{3.5b}$$

Therefore, once $J'_N Z_0$ is known, the impedances and thus the dimensions of the N-th coupled line section can be obtained.

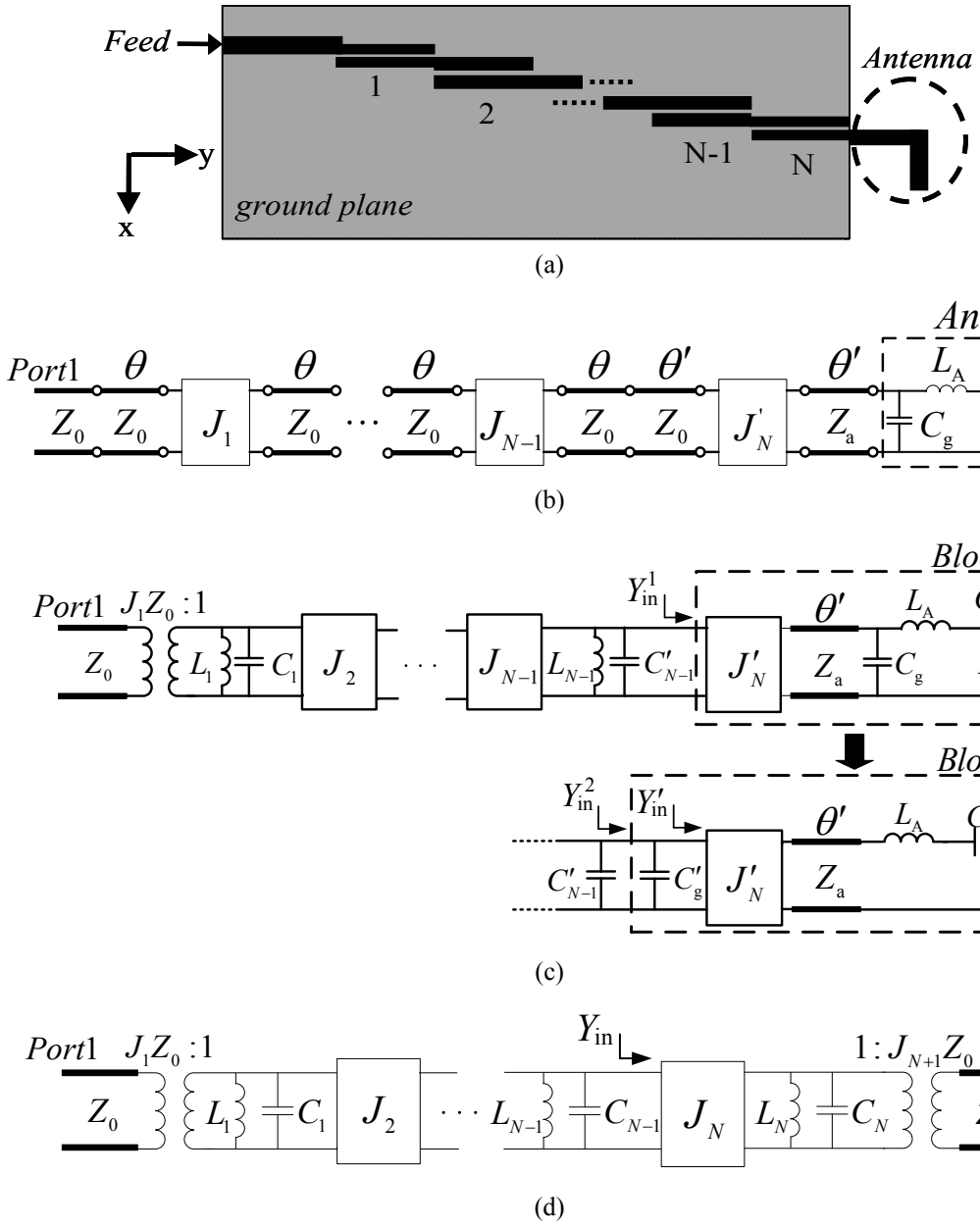

Figure 3.8 (a) The structure of the proposed *N*-order filtering antenna. (b) Equivalent circuit of the proposed filtering antenna. (c) Modified circuit of the proposed filtering antenna. (d) A typical *N*-order bandpass filter circuit using shunt resonators with admittance inverters.

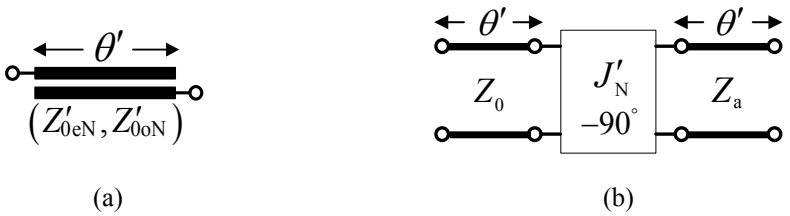

Figure 3.9 (a) Geometry of the *N*-th coupled line section and (b) the corresponding equivalent circuit.

By using the equivalent circuits of the antenna and the coupled line sections, the filtering antenna structure shown in Figure (a) can be expressed by the equivalent circuit shown in Figure (b). The two transmission line sections in between the admittance inverters have lengths equal to a half wavelength near the center frequency, i.e., $2\theta \approx \theta+\theta' \approx \pi$, and thus can be replaced by a parallel *LC* resonator as shown

in the upper sub-figure of Figure (c). To transfer this circuit to a typical bandpass filter topology, the antenna's parasitic capacitance C_g should be moved to the left-hand side of the admittance inverter J'_N as illustrated in Block 2 of Figure (c). The resultant capacitance C'_g can be derived by equalizing the input admittances of Blocks 1 and 2 in the figure. For frequencies near f_0 and $\theta' \approx \pi/2$, the input admittance Y^1_{in} of Block 1 and Y^2_{in} of Block 2 can be derived and approximated as

$$Y^1_{in} \approx J'^2_N Z^2_a \left(j2\pi f C_g + \frac{1}{j\sqrt{\frac{L_A}{C_A}}\left(\frac{f}{f_0} - \frac{f_0}{f}\right) + R_A} \right) \tag{3.6}$$

$$Y^2_{in} = j2\pi f C'_g + Y'_{in} \tag{3.7}$$

with

$$Y'_{in} \approx \frac{J'^2_N Z^2_a}{j\sqrt{\frac{L_A}{C_A}}\left(\frac{f}{f_0} - \frac{f_0}{f}\right) + R_A} \tag{3.8}$$

By equalizing (3.6) and (3.7), one obtains

$$C'_g = (J'_N Z_a)^2 C_g \tag{3.9}$$

Actually, the capacitance C'_g is much smaller than C'_{N-1}, therefore, the total capacitance C_{N-1} $(=C'_{N-1}+C'_g)$ of the second resonator is approximately equal to C'_{N-1}.

Finally, the equivalent circuit of Figure (c) can be transferred to the conventional N-th order bandpass filter circuit as shown in Figure (d), and, by letting the admittance Y'_{in} equal Y_{in}, one obtains

$$Q_A = \frac{2\pi f_0 L_A}{R_A} = \frac{\pi}{2(Z_0 J_{N+1})^2} \tag{3.10}$$

and

$$J'_N Z_0 = \frac{J_N Z_0}{Z_a}\left(\frac{2Q_A R_A Z_0}{\pi}\right)^{1/2} \tag{3.11}$$

The design procedures of the proposed filtering antenna can now be summarized as follows:

1) Specify the requirements of the bandpass filter to be synthesized, including the center frequency f_0, the fractional bandwidth Δ, and the type of the filter (e.g., bandpass filter with equal ripple), from which the admittance inverters J_nZ_0 (n = 1, 2, …, N+1) and the parallel resonators L_n, C_n (n = 1, 2, …, N) in Figure (d) can be determined [47].
2) Choose an antenna structure with suitable equivalent circuit that can substitute for the last resonator and

load impedance of the bandpass filter. (Here in this study, the inverted-L antenna is used.) And then get a database associated with the equivalent circuit components for different antenna dimensions like those in Section 3.1.1.

3) Calculate the antenna quality factor Q_A from (3.10) and then, after choosing a suitable strip width (e.g., the same width as the feed line), obtain the required strip length l_1 and radiation resistance R_A of the inverted-L antenna by using Figure . The length l_2 of the horizontal antenna strip can thus be determined by letting the antenna resonate at f_A. At this step, the dimensions of the inverted-L antenna are acquired.

4) Choose suitable characteristic impedance Z_a and then calculate the inverter constant $J'_N Z_0$ by using (3.11). Following, the even- and odd-mode characteristic impedances Z'_{0eN} and Z'_{0oN} of the N-th coupled line section for the proposed filtering antenna can be attained via (3.5).

5) Calculate the even- and odd-mode characteristic impedances Z_{0en} and Z_{0on} (n = 1, 2, …, N-1) of the coupled line sections by using the formulae in [47], and then all the dimensions of the N coupled line sections in the proposed filtering antenna can be determined.

3.2.2 Design Examples and Experimental Verificatio

In this section, an example of the proposed filtering antenna is to be presented. Following the above design procedures, a third-order Chebyshev bandpass filter with a 0.1 dB equal- ripple response, f_0 = 2.45 GHz, Δ = 14%, and Z_0 = 50 Ω are firstly chosen. Based on these requirements, the inverter constants $J_n Z_0$ (n = 1 ~ 4) of the bandpass filter can be calculated. Also, these parallel resonators in Figure (d) have the values of (L_n, C_n) = (2.068 nH, 2.041 pF), where n = 1, 2, and 3. Then, with a strip width w = 1.17 mm, the quality factor Q_A = 7.37 is obtained by using (3.10). This corresponds to a strip length l_1 = 10 mm from the Q_A–to-l_1 relationship shown in Figure . To this point, all the dimensions of the inverted-L antenna are gotten, that is, l_1 = 10 mm, l_2 = 17.25 mm, and w = 1.17 mm. Hence, the radiation resistance R_A can be found as 28.6 Ω via Figure .

Following, the inverter constant $J'_3 Z_0$ of the third coupled line and thus the even- and odd-mode characteristic impedances Z'_{0e3} and Z'_{0o3} can be calculated by using (3.11) and (3.5), respectively, from which the line width and the gap between lines of the third coupled line are obtained. Note that these dimensions are dependent on the characteristic impedance Z_a used in the synthesis of the filtering antenna. Figure depicts their variations as functions of Z_a. It is seen that the larger is the impedance Z_a, the smaller the gap size is. When Z_a > 50 Ω, the gap would become smaller than 0.1 mm, which is difficult to realize. Thus, for easy fabrication, a characteristic impedance of Z_a = 30 Ω is selected here. This would correspond to an inverter constant $J'_3 Z_0$ = 0.5515 and even- and odd-mode characteristic impedances (Z'_{0e3}, Z'_{0o3}) = (75.67 Ω, 42.58 Ω). Finally, the even- and odd-mode characteristic impedance of the first and second coupled line sections are calculated, and then all dimensions of each coupled line section for the proposed filtering antenna can be obtained. It should be noted that the gap size of the first coupled line section is extremely small and difficult to fabricate. To tackle this problem, the tapped structure with a quarter-wavelength impedance transformer [53] is utilized, as shown in Figure 3.7.

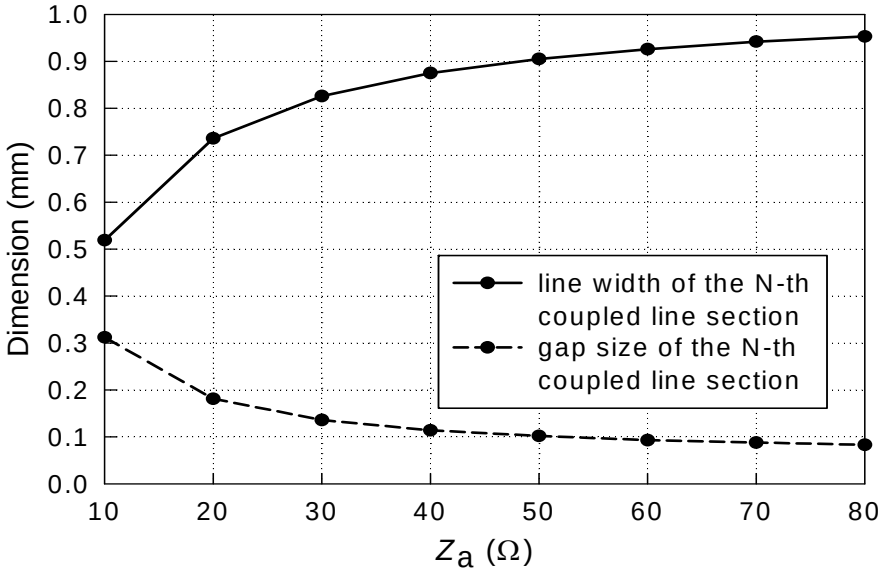

Figure 3.10 Dimensions of the third coupled line section for different Z_a in the proposed filtering antenna.

The full-wave simulated return loss of the proposed filtering antenna in comparison with that of the conventional third-order Chebyshev bandpass filter is shown in Figure (a). The simulated return loss of a second-order bandpass filter directly cascaded with a 50 Ω inverted-L antenna is also shown for reference. It is noticed that both of the proposed filtering antenna and filter directly cascaded with an antenna are third-order circuit, with two orders provided by the circuit and one by the antenna. These two structures occupy about the same circuit area. Here, the conventional third-order Chebyshev bandpass filter has the same specifications as the filtering antenna (14% bandwidth and 0.1 dB equal-ripple response). And the filter in the reference structure is a second-order Chebyshev bandpass filter with the same bandwidth and ripple level. It is observed that the bandwidth and skirt selectivity for the proposed filtering antenna agree very well with the conventional third-order Chebyshev bandpass filter, which demonstrates the design validity of the filtering antenna. On the other hand, putting an individually designed antenna after the bandpass filter via a simple cascaded 50 Ω microstrip line, not only have no contribution to the order of the filter, but also deteriorate the original filter performance, especially resulting in bad skirt selectivity at the band edges.

Figure (b) compares the measured return losses of the proposed filtering antenna and the conventional third-order Chebyshev bandpass filter. The simulated return loss of the filtering antenna is also shown for comparison. Likely because of the deviations in dielectric constant and substrate thickness, the bandwidth of the measured return loss of the proposed filtering antenna is slightly narrower than the simulated one. However, it is in close agreement with the measured one of the conventional third-order Chebyshev bandpass filter. Both have the same passband poles' positions, the selectivity at the band edge, and the return-loss behavior at the stopband. This demonstrates that the proposed filtering antenna has good selectivity in accordance with the conventional bandpass filter.

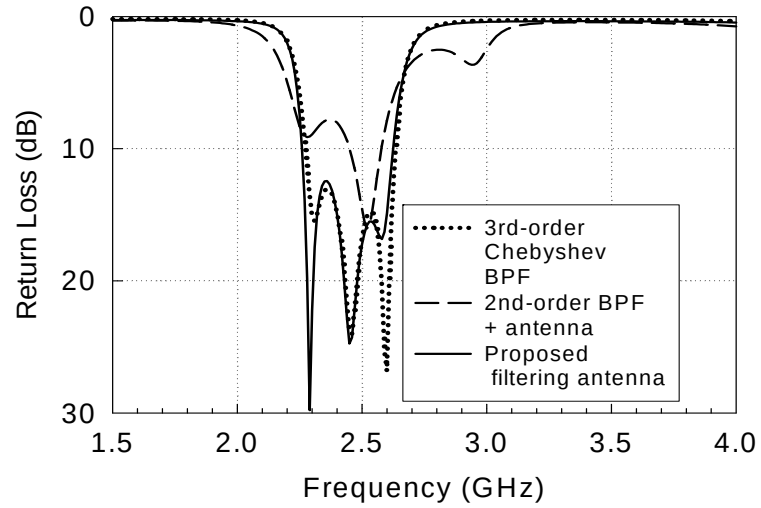

(a)

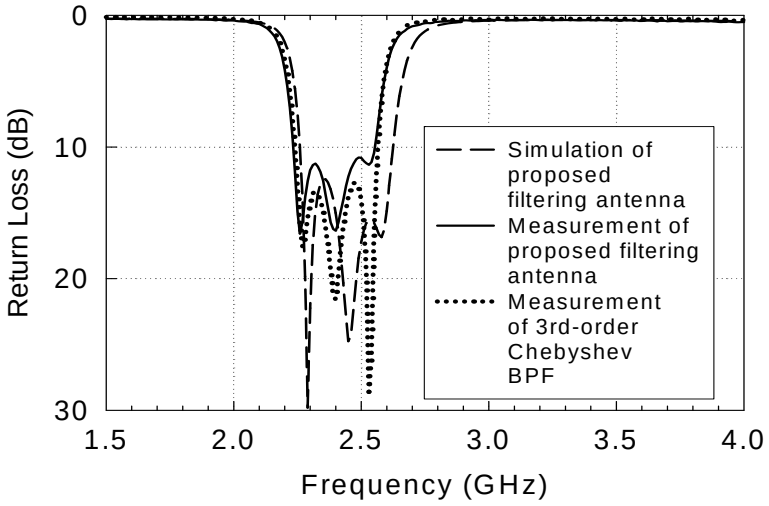

(b)

Figure 3.11 (a) Full-wave simulated return losses of the proposed filtering antenna, 2nd-order BPF + antenna, and the conventional 3rd-order Chebyshev BPF. (b) Measured return loss of the proposed filtering antenna compared with the measured one of the conventional 3rd-order Chebyshev BPF.

Figure 3.12(a) shows the full-wave simulated total radiated powers of the proposed filtering antenna and the reference structure of a 2nd-order filter directly cascaded with antenna. Here, the total radiated power has been normalized to the input power. The simulated insertion loss of the conventional third-order Chebyshev bandpass filter is also shown for comparison. As compared to the reference structure, the total radiated power of the proposed filtering antenna is flat in the passband and the bandwidth is very close to the insertion-loss bandwidth of the third-order Chebyshev bandpass filter. The measured total radiated power of the proposed structure, which is in close agreement with the simulated one expect for the deviations of the bandwidth, is also shown in Figure 3.12(a).

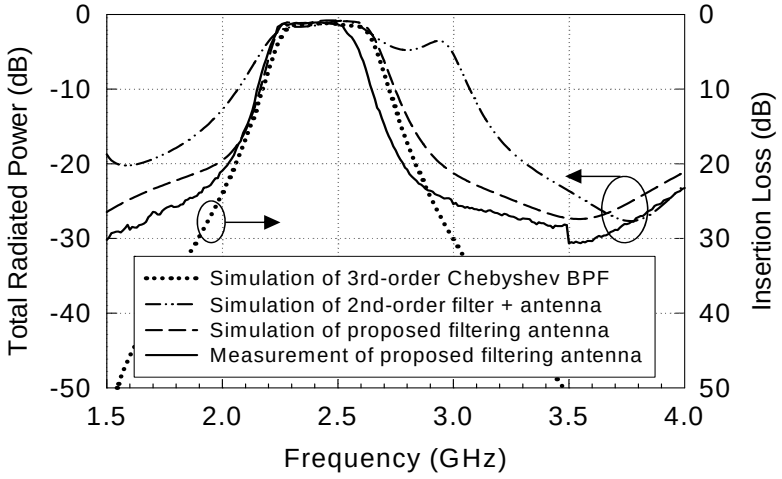

(a)

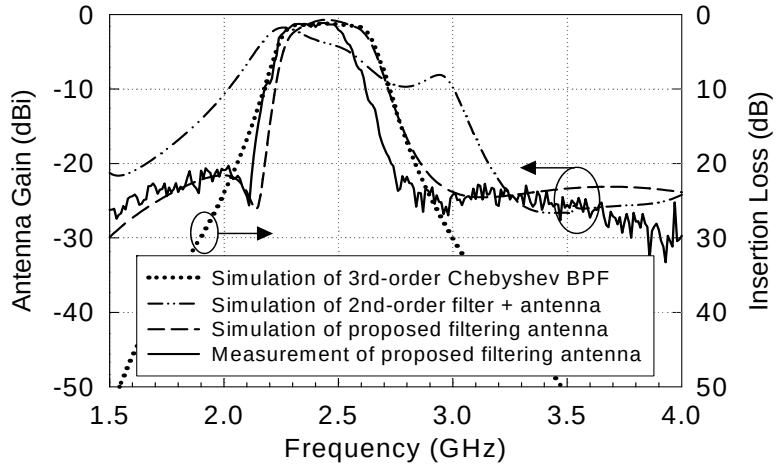

(b)

Figure 3.12 (a) Full-wave simulated and measured total radiated power compared with the simulated insertion loss of the conventional 3rd-order Chebyshev BPF. (b) Simulated and measured antenna gains versus frequency in the +*z* direction compared with the simulated insertion loss of the conventional 3rd-order Chebyshev BPF.

Figure 3.12(b) shows the full-wave simulated antenna gains in the +*z* direction versus frequency for the proposed filtering antenna and the reference structure of a 2nd-order filter directly cascaded with antenna. The simulated insertion loss of the conventional third-order Chebyshev bandpass filter is also shown for comparison. Since the inverted-L antenna has an omni-directional field pattern in the *xz*-plane, has only the antenna gain in the +*z* direction is discussed. As compared to the reference structure, the antenna gain of the proposed filtering antenna is flat in the passband and the bandwidth is very close to the insertion-loss bandwidth of the third-order Chebyshev bandpass filter. The proposed filtering antenna also provides better skirt selectivity with stopband suppression better than 22 dB. The measured antenna gains for the proposed filtering antenna is also depicted in Figure 3.12(b), which shows an antenna gain, including the circuitry loss, of -1.3 dBi. It is obvious that the measurement matches well to the simulation. The amplitude noise of the measured gain in the stopbands is due to the system noise of the antenna chamber.

In Figure 3.12(b), a radiation null at f = 2.15 GHz in the +*z* direction, which makes the skirt selectivity better than that of the conventional bandpass filter, has been observed. Since an inverted-L antenna alone should exhibit a monotonous gain dropping, but not a local gain minimum when the operating frequency moves away from the antenna's resonant frequency. Also, since it has been found that the frequency

locations of these nulls depend on the observation angle, they are not caused by the circuit coupling between the first resonator and the third one (i.e., the inverted-L antenna) of the filter. It is finally found out that the last coupled line structure near the ground edge of the proposed filtering antenna induces a strong spurious ground edge current, which in turn produces extra radiation and cancels the radiation field from the antenna at some frequency. Figure 3.13 shows the simulated radiation patterns in the *xz*-plane at $f = 2.15$ GHz for the proposed filtering antenna and a two-port circuit structure obtained from the filtering antenna with the inverted-L section replaced by a terminated port. It is seen that the two-port circuit produces a spurious radiation toward $+z$ direction with peak gain about -14 dBi, which is the same level as the omni-directional field pattern of an inverted-L antenna after the attenuation of the third-order bandpass filter at $f = 2.15$ GHz. For field canceling, the total radiation pattern of the filtering antenna thus possesses a radiation null near the $+z$ direction.

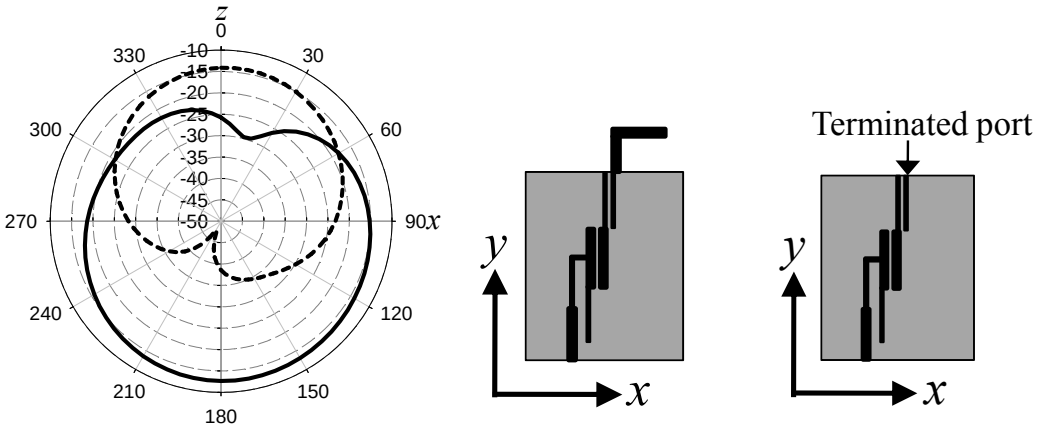

Figure 3.13 Full-wave simulated total-field radiation patterns in the *xz* plane at $f = 2.15$ GHz for the proposed filtering antenna and a two-port circuit structure obtained from the filtering antenna with the inverted-L section replaced by a terminated port. [solid line: proposed filtering antenna; dashed line: two-port circuit structure.]

The measured and simulated total-field radiation patterns at $f_0 = 2.45$ GHz in the three principal planes are also presented in Figure 3.14. It is seen that the measured patterns are similar to the simulated ones, although a discrepancy occurs at $\theta = 180°$ in the *yz*- and *xz*-planes (that is, the $-z$ direction) due to the interference of the feeding coaxial cable in the measurement. The radiation pattern in the *xz*-plane is nearly omnidirectional with peak gain of 0.65 dBi. Figure 3.15 shows the photographs of the proposed filtering antenna compared with a second-order bandpass filter directly cascaded with an inverted-L antenna.

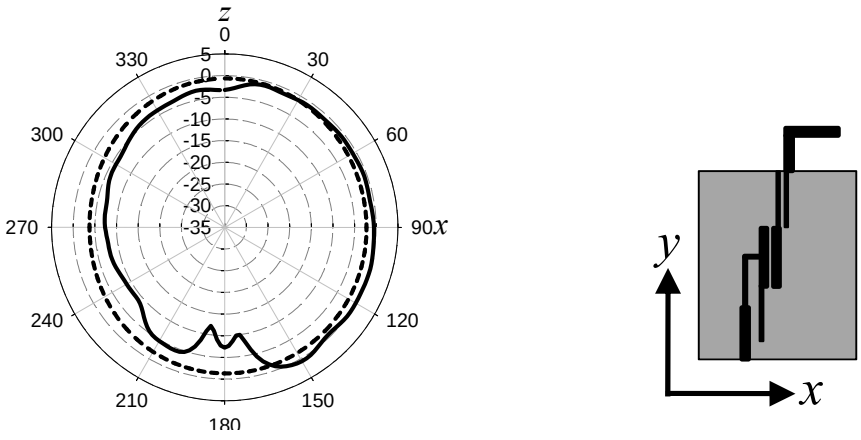

(a)

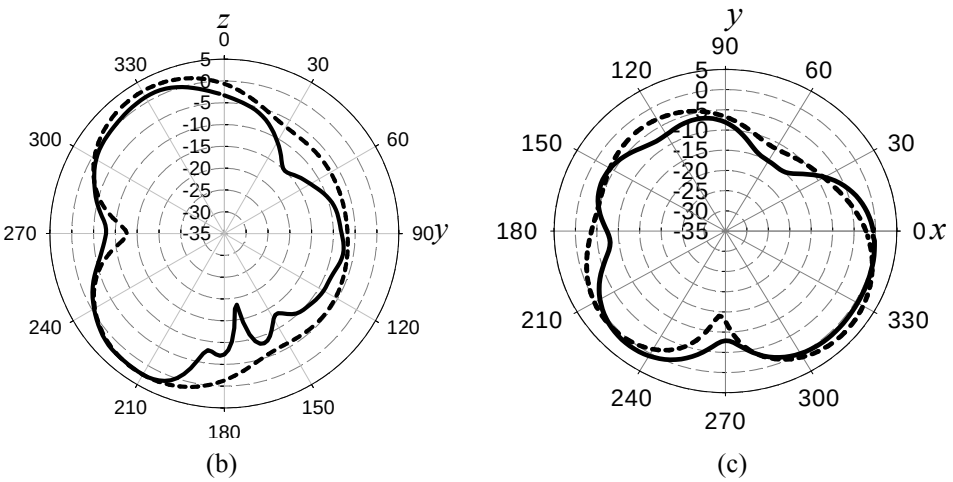

Figure 3.14 Measured and simulated total-field radiation patterns in the (a) *xz*, (b) *yz*, and (c) *xy* planes for the proposed filtering antenna. [solid line: measured results; dashed line: full-wave simulated results]. f_0 = 2.45 GHz.

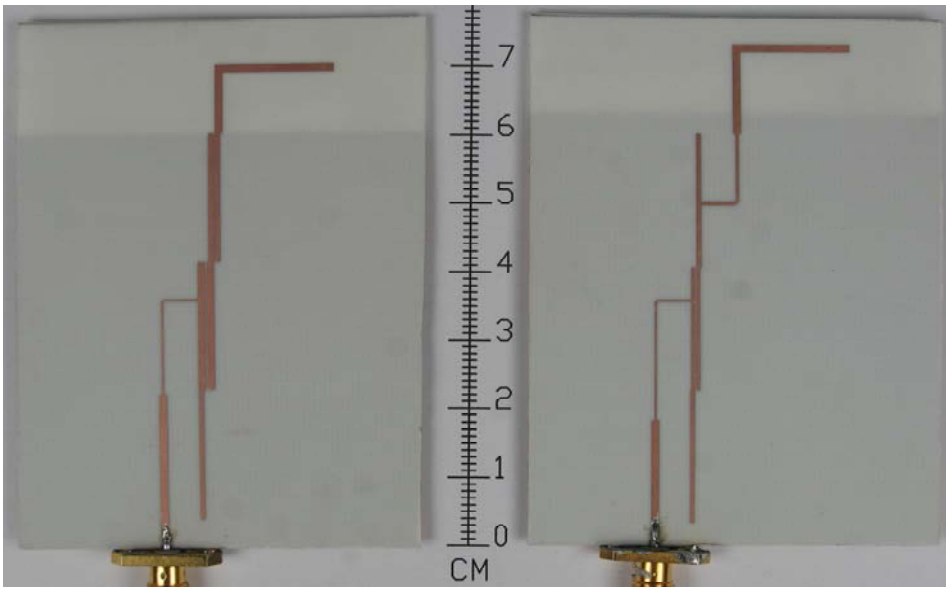

Figure 3.15 Photographs of the proposed filtering antenna (left-side) and 2nd-order BPF + antenna (right-side).

3.3 Compact Printed Filtering Antennas Using a Ground-Intruded Coupled Line Resonator

In this section, the compact printed filtering antennas with high band-edge gain selectivity are presented, as shown in Figure 3.16. Occupying about the same substrate area as a conventional antenna, the proposed structure not only serves as a radiator but also a second-order bandpass filter, with one filter pole provided by an antenna and the other by a newly proposed coupled line resonator. High band-edge selectivity is achieved due to two additional stop-band transmission zeros provided by the coupled line resonator. To minimize the required area and reduce the spurious radiation, a coupled line structure composed of a microstrip line and a coplanar waveguide by broadside coupling is adopted and intruded into an antenna area. According to the filter specifications, a design procedure for the proposed filtering antenna is depicted in detail. As compared

to the conventional antenna, the proposed filtering antenna not only possesses a similar antenna gain but also provides better band-edge gain selectivity and flat passband gain response.

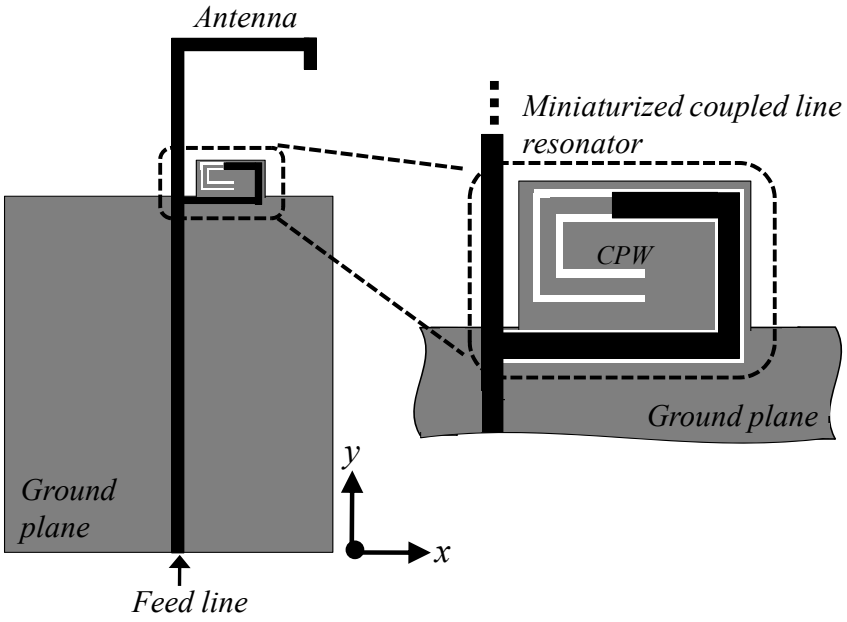

(a)

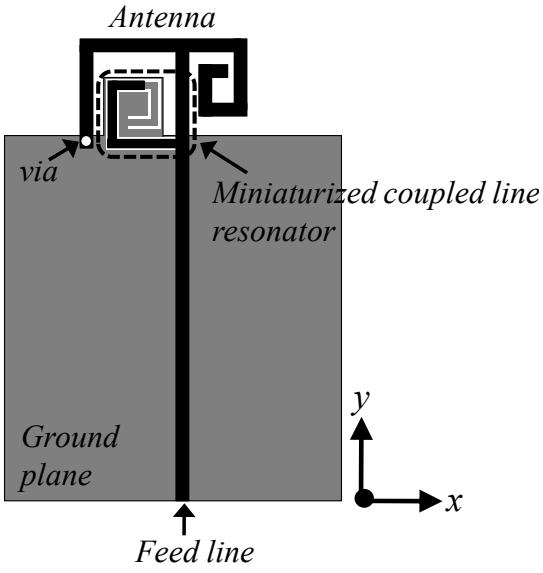

(b)

Figure 3.16 The proposed compact second-order filtering antenna is composed of a miniaturized coupled line resonator and (a) a Γ–shaped antenna, (b) a spiraled inverted-F antenna.

3.3.1 Synthesis of the Filtering Antenna

In this section, the synthesis of a filtering antenna by using the coupled line resonator, which has been discussed in Section 2.1, is to be presented. The proposed filtering antenna is constructed by directly connecting the coupled line resonator to a Γ–shaped antenna, as shown in Figure 3.17(a). Since the antenna is a variety of a monopole antenna, it has a series *RLC* equivalent circuit as shown in Figure 3.17(b) [45]. Here, L_A and C_A express the equivalent inductance and capacitance, respectively, and R_A corresponds to the antenna radiation resistance. It is noted that an extra shunt capacitance C_g is incorporated in the equivalent

circuit here so that the whole circuit would have the same impedance behavior as the antenna itself in a wider frequency range, as depicted in Section 3.1.1. This parasitic capacitance comes from the accumulation of charges around the antenna feed point due to the truncation of the ground plane.

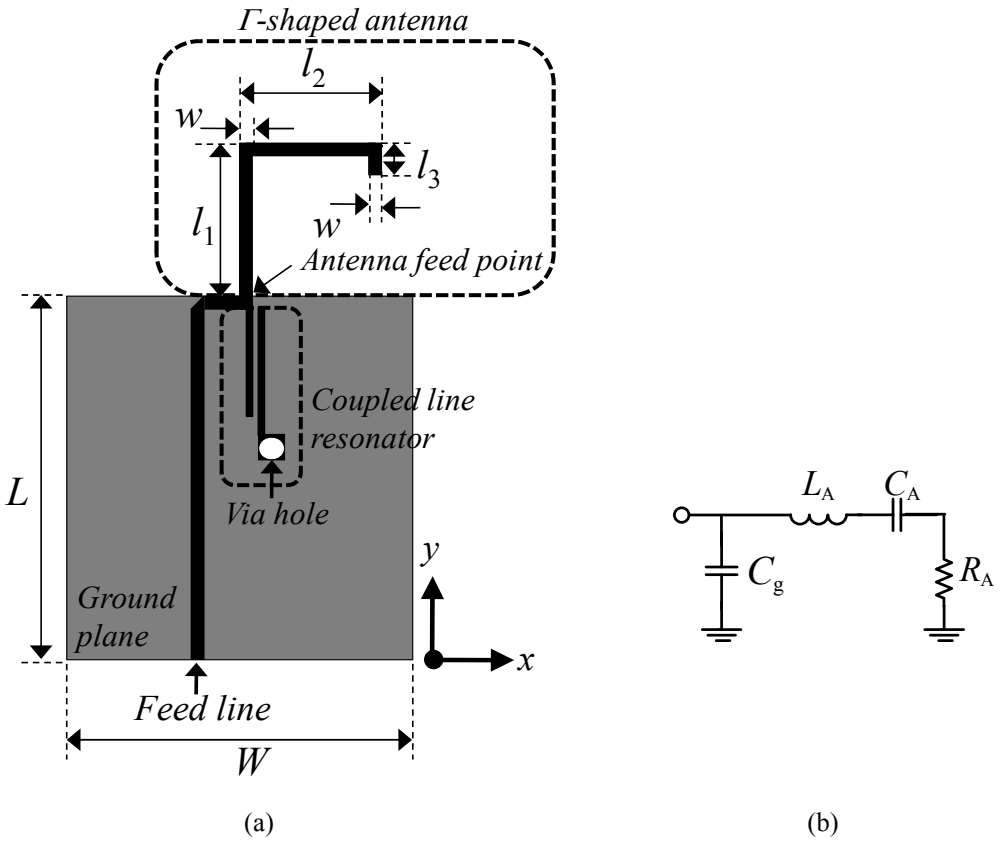

Figure 3.17 (a) The geometry of the second-order filtering antenna. (b) The corresponding equivalent circuit of the Γ–shaped antenna.

By using the equivalent circuits of the coupled line resonator and the Γ–shaped antenna, the second-order filtering antenna can be expressed by the equivalent circuit shown in Figure 3.18(a). It can be observed that not only second-order response but also two extra transmission zeros near the filter's band-edge can be produced. Figure 3.18(b) is a further equivalent circuit of the filtering antenna while the resonant frequency of the coupled line resonator is near f_r. This circuit can then be transformed to a typical second-order bandpass filter as shown in Figure 3.18(c), where $L_2 = L_A$, $C_2 = C_A$, $R_0 = R_A$, and $C_1' = C_1 + C_g$. Note that due to the existence of the small capacitance C_g, the required resonant frequency f_r ($= \left(2\pi\sqrt{L_1 C_1}\right)^{-1}$) of the coupled line resonator is slightly larger than the operating frequency f_0 ($= \left(2\pi\sqrt{L_1 C_1'}\right)^{-1} = \left(2\pi\sqrt{L_2 C_2}\right)^{-1}$) of the bandpass filter.

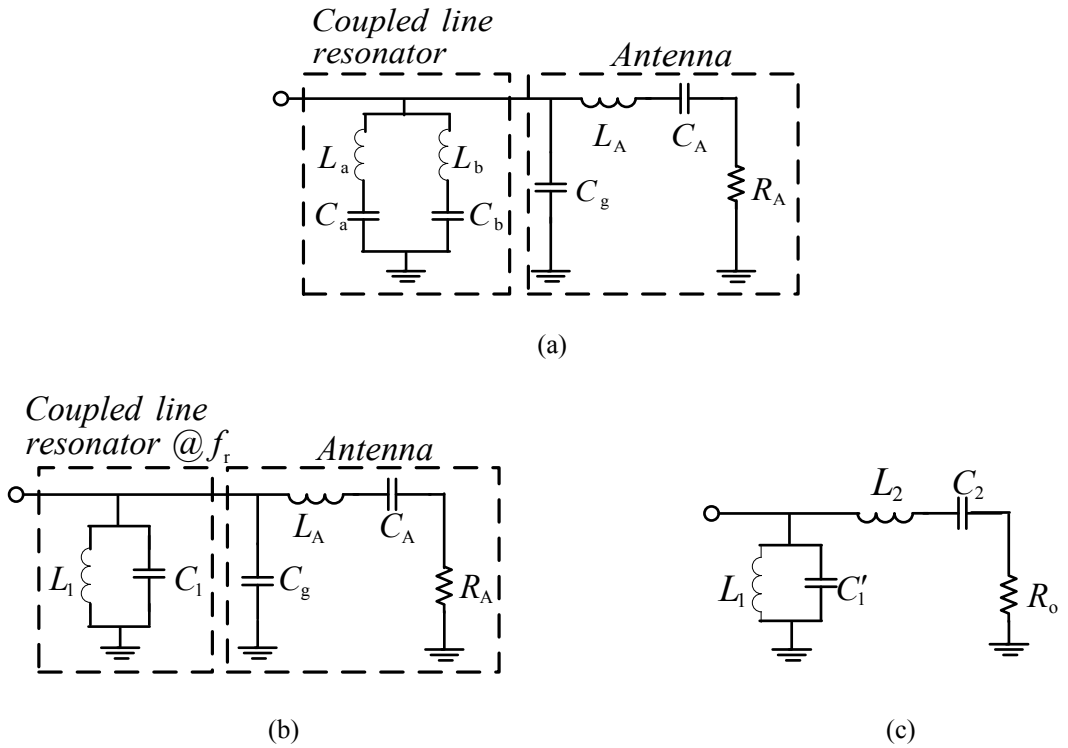

Figure 3.18 (a) Equivalent circuit of the second-order filtering antenna. (b) Equivalent circuit of the filtering antenna while the resonant frequency of the coupled line resonator is near f_r. (c) Equivalent circuit of the typical second-order bandpass filter.

The design procedures of the proposed filtering antenna are listed below:

1) Specify the requirements of the bandpass filter to be synthesized, including the operating frequency f_0, the frequencies of the transmission zeros (f_a and f_b), the fractional bandwidth Δ, and the type of the filter (e.g., bandpass filter with equal ripple). Therefore, the circuit elements (L_2, C_2, R_0, L_1, C_1') of the typical bandpass filter in Figure 3.18(c) can be calculated [47].
2) Choose the suitable dimensions of the Γ-shaped antenna and then extract the circuit elements (L_A, C_A, R_A, C_g) of its equivalent circuit as in Section 3.1.1. These circuit elements are used to function as the last (second) stage of the filter. Therefore, the antenna dimensions should be determined so as to satisfy the following requirements: $L_A = L_2$, $C_A = C_2$, and $R_A = R_0$.
3) Use the component values of L_1, $C_1 (= C_1' - C_g)$ obtained in the above procedures, together with the required resonant frequencies f_r $\left(= \left(2\pi\sqrt{L_1 C_1}\right)^{-1} \right)$ and lower transmission zero f_a, the characteristic impedances (Z_{0e}, Z_{0o}) of the coupled line resonator with equal lengths can be calculated by using (2.5), and then its corresponding dimensions can be obtained.
4) Properly shorten the open stub's length (θ_1) in the coupled line resonator with unequal lengths so as to adjust the higher transmission zero to the required one (f_b). Note that although the position of the lower transmission zero is changed in this step, the variation is quite limited as shown in Figure 2.4(a). If a more precise lower transmission zero is required, the frequency f_a used in the above procedure can be set a little smaller than the required one to compensate the effect when shortening the stub's length.

As an example, a second-order Chebyshev bandpass filter with a 0.1 dB equal-ripple response is tackled. The filtering antenna is designed on a 0.508 mm thick Rogers 4003 substrate with a dielectric constant of 3.38

and loss tangent of 0.0027. The ground plane size $L \times W$ = 50 mm×50 mm. In the design, the full-wave simulation solver HFSS [51] is used for fine tuning in the last procedure. According to the design procedure, the specifications of the filter should be firstly chosen. Here, the bandpass filter has a operating frequency f_0 = 2.45 GHz, a fractional bandwidth Δ = 14%, and Z_0 = 50 Ω. The lower transmission zero f_a is set at 2 GHz, and the higher transmission zero f_b is 3.3 GHz. Based on these requirements, the circuit components of the filter can be calculated, which are L_1 = 0.54 nH, C_1' = 7.82 pF, L_2 = 14.43 nH, C_2 = 0.29 pF, and R_0 = 37 Ω. Secondly, we have to determine the antenna sizes. After numerous simulations, we choose the dimensions of the Γ-shaped antenna as l_1 = 15.2 mm, l_2 = 11.5 mm, l_3 = 3.1 mm, and w = 1.17 mm, which correspond to a set of extracted component values (i.e., L_A = 14.4 nH, C_A = 0.29 pF, R_A = 37 Ω, C_g = 0.37 pF) nearest to required one.

Thirdly, the circuit component C_1 and the resonant frequency f_r of the coupled line resonator are calculated, which are 7.45 pF and 2.51 GHz, respectively. The characteristic impedances (Z_{0e}, Z_{0o}) = (89 Ω, 47 Ω) can then be gotten by using (2.5) and the given lower transmission zero, with which the dimensions of the coupled line resonator of equal lengths are obtained. The resultant line width, gap size, and length of the coupled line are 0.64 mm, 0.15 mm, and 18.9 mm, respectively. Finally, to reach a transmission zero at 3.3 GHz, the electric length θ_1 of the open-circuited stub is shortened from $90°$ to $70°$ by simulation. To this end, all the structure dimensions have been determined. And the filtering antenna can be implemented by connecting the coupled line resonator and the Γ-shaped antenna, as shown in Figure 3.17(a).

Figure 3.19(a) shows the full-wave simulated return loss of the designed filtering antenna. The simulated result of the Γ–shaped antenna only is also shown for reference. The proposed filtering antenna exhibits a return loss larger than 15 dB over the passband, and provides better band-edge selectivity as compared to the Γ–shaped antenna only. Also observe that, with the center frequency at 2.45 GHz, the filtering antenna possesses two transmission poles at 2.33 GHz and 2.57 GHz, which are caused from the repel of resonant frequencies due to mutual coupling between the coupled line resonator and Γ–shaped antenna [54]. Although not shown here, it has been found that the lower and higher transmission poles can be tuned independently by the coupled line resonator and the antenna, respectively.

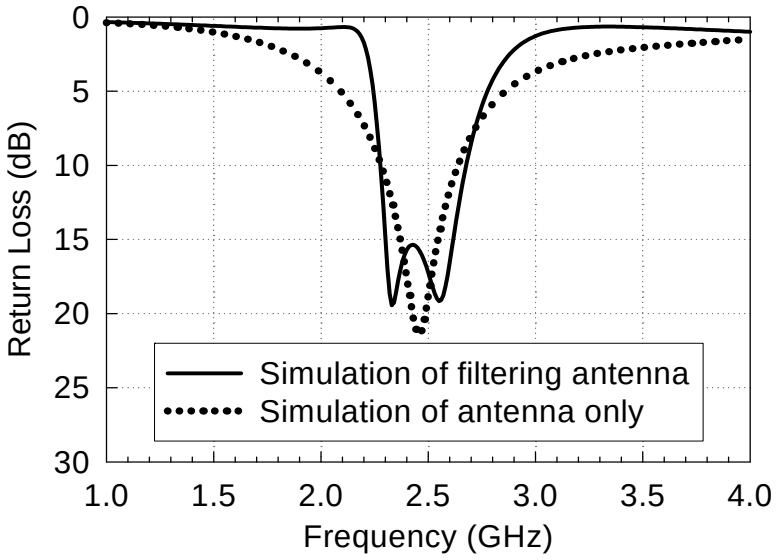

(a)

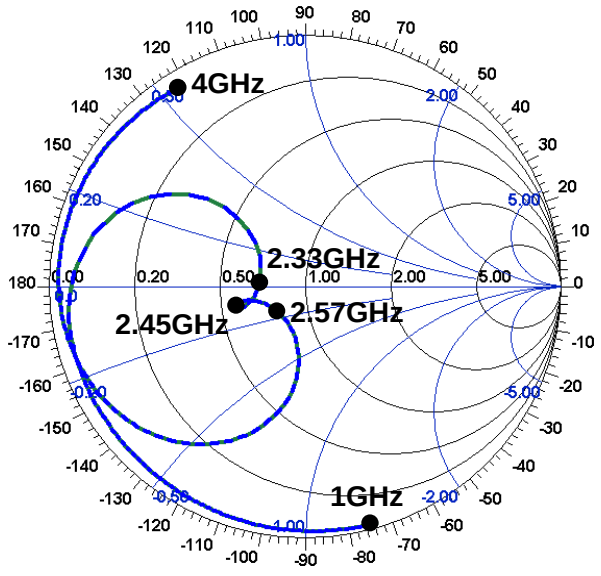

(b)

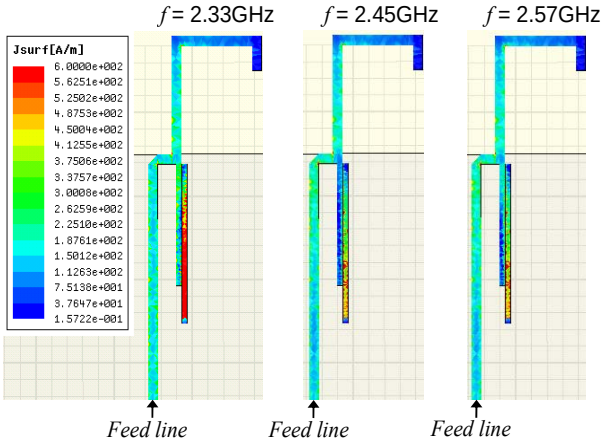

(c)

Figure 3.19 (a) The full-wave simulated return loss of the filtering antenna in comparison with the simulated one of the Γ-shaped antenna. (b) The impedance behaviour on the Smith chart of the filtering antenna. (c) The simulated current distributions of the filtering antenna at the center frequency and two transmission poles.

Figure 3.19(b) depicts the impedance behaviour on the Smith chart of the filtering antenna, and Figure 3.19(c) illustrates the current distributions at the center frequencies and the two transmission poles. At these three in-band frequencies, as observed from Figure 3.19(b), the input impedance possesses negligible reactance but has similar resistances around 30 Ω. Due to the high radiation efficiency in the passband, the input resistance of the proposed antenna is nearly equal to the radiation resistance. Consequently, the currents distributed on the Γ–shaped antenna have about the same level at these frequencies, as can be observed from Figure 3.19(c). Also notice from Figure 3.19(c) that the current on the coupled line resonator at 2.33 GHz is relatively large as compared to those at 2.45 GHz and 2.57 GHz, which is apparent since the coupled line resonator is the main contributor for the lower transmission pole at 2.33 GHz.

Figure 3.20 shows the full-wave simulated total radiated power of the filtering antenna in comparison with the simulated one of the Γ–shaped antenna. Here, the total radiated power has been normalized to the input power. It is seen that the filtering antenna exhibits a constant radiation power over the required frequency bandwidth, and has two radiation nulls at 2.13 GHz and 3.33 GHz which are close to the design ones. Also, the proposed filtering antenna has much better stop-band suppression and band-edge selectivity. The corresponding radiation efficiency of the filtering antenna is about 88% in the passband, but is greatly reduced to 0.9% and 0.7% at the frequencies of the two radiation nulls. The input power is mostly reflected back due to the low return losses (about 0.7 dB) at these two nulls.

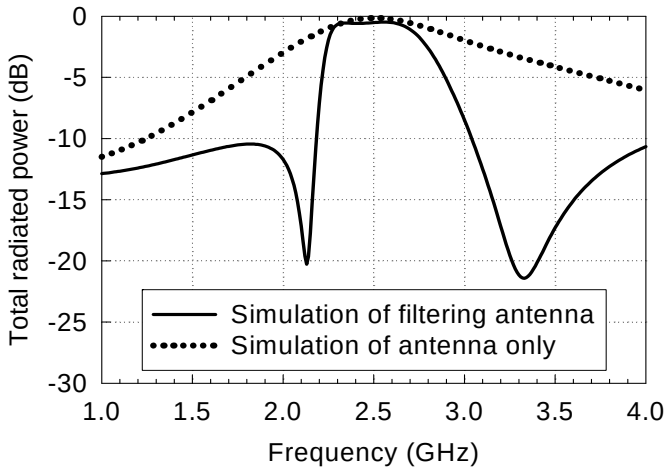

Figure 3.20 The full-wave simulated total radiated power of the filtering antenna in comparison with the simulated ones of the Γ-shaped antenna.

3.3.2 Compact Second-Order Filtering Antenna I

Although the proposed filtering antenna shown in Figure 3.17(a) exhibits good radiation and filtering performances, it still occupies extra circuit area due to the use of the coupled line resonator. To realize a compact filtering antenna, a miniaturized coupled line resonator composed of a microstrip line open-circuited stub and a coplanar waveguide short-circuited stub by broadside coupling is proposed, as shown in Figure 3.21, to intrude into the Γ-shaped antenna area. Herein, an extended ground plane ($W_1 \times L_1$) is employed for designing the folded coupled line resonator.

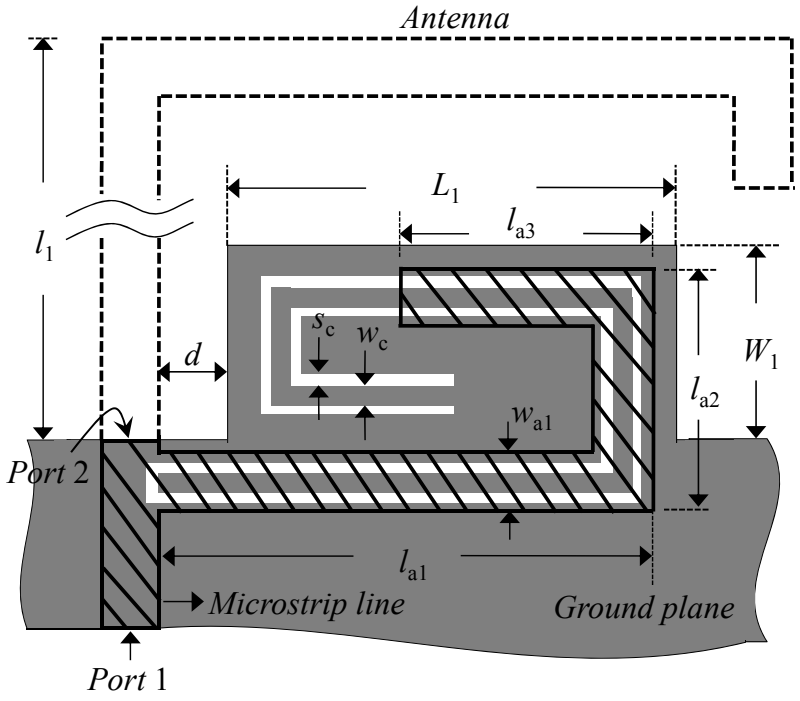

Figure 3.21 Geometry of the proposed miniaturized coupled line resonator in the compact filtering antenna. I.

Figure 3.22 shows the full-wave simulated scattering parameters for different dimensions of the miniaturized coupled line resonator. Note that the simulation result does not include the effect of the Γ-shaped antenna. It considers only the two-port folded coupled line resonator between ports 1 and 2 (see Figure 3.21). The size ($W_1 \times L_1$) of the extended ground plane is 3.4 × 7.5 mm^2 and the distance d between the extended ground plane and vertical strip line (l_1) of the Γ-shaped antenna is 1mm. Figure 3.22(a) depicts the effect of the length l_{a3} of the microstrip line open-circuited stub. The coplanar waveguide short-circuited stub has a fixed total length of about a quarter wavelength and a line width w_c = 0.3 mm and gap s_c = 0.2 mm. As shown, the miniaturized resonator has the same properties as the original one (Fig. 2.1 (b) in Section 2.1). It possesses a transmission pole and two side transmission zeros. Also, when the open-circuited stub is shortened (i.e., decreasing l_{a3}), the behavior near the center frequency is unchanged, and the two transmission zeros move toward the higher frequencies, with the higher transmission zero moving faster than the lower one.

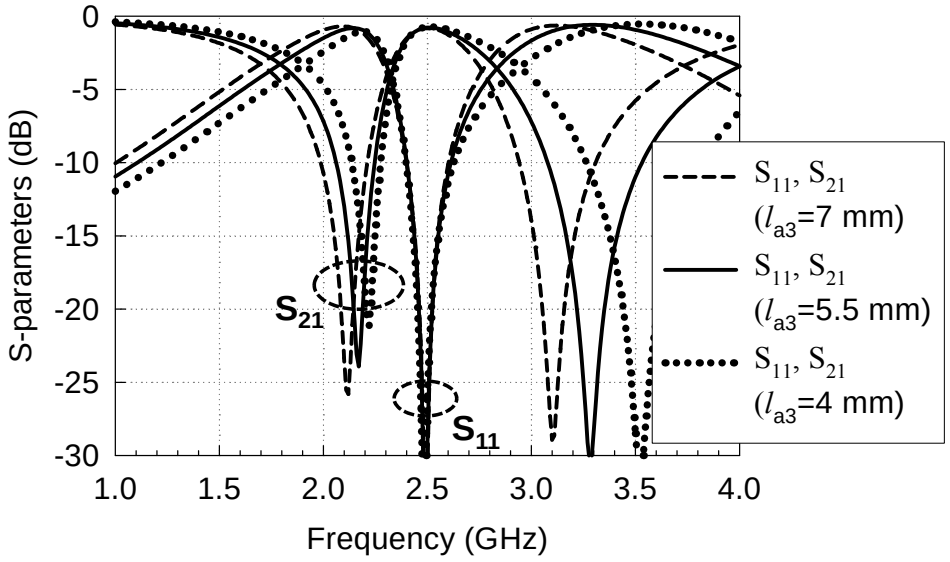

(a)

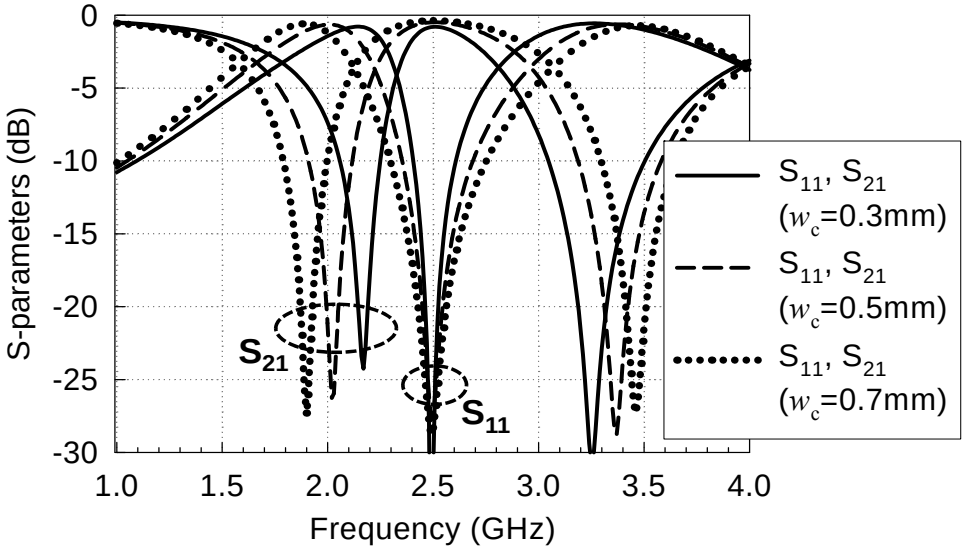

(b)

Figure 3.22 Full-wave simulated S-parameters of the miniaturized coupled line resonator with unequal lengths. (a) different l_{a3} with w_c = 0.3 mm. (b) different w_c with l_{a3} = 5.5mm. (w_{a1} = 1.2mm, S_c = 0.2 mm and f_r = 2.5 GHz)

Figure 3.22(b) illustrates the effect of the line width w_c of the coplanar waveguide stub. As w_c increases, the center frequency remains the same due to the same short-circuited stub length ($\lambda/4$). While the two transmission zeros move away from the center frequency. This is because the increase of w_c causes a stronger mutual coupling between the microstrip line and the coplanar waveguide, which thus results in a larger ratio of Z_{0e}/Z_{0o}. Therefore, from (2.2c) and (2.2d), the lower transmission zero appears at a lower frequency and the higher zero at a higher frequency.

In summary, the intruded miniaturized coupled line resonator follows the behaviors depicted in Section 2.1. Thus, the design methodology described in the previous section can be applied directly to the proposed compact filtering antenna (Figure 3.16(a)). In the design, the filter specifications to be achieved and the dimensions of the Γ–shaped antenna are set the same as those in Section 3.3.1. And the final dimensions of the miniaturized coupled line resonator are listed in Table 3.1. Figure 3.23(a) and (b) shows the full-wave simulated and measured return losses and total radiated powers, respectively, of the compact filtering antenna. The simulated results of the Γ–shaped antenna are also shown for reference. It is seen that the full-wave simulated results of the compact filtering antenna are almost the same as those of the original design (Figure 3.17(a)), which show two filter poles at 2.3 GHz and 2.6 GHz and two radiation nulls at 2.11 GHz and 3.31 GHz. The simulated radiation efficiency at operating frequency $f_0 = 2.45$ is about 82%, slightly lower than the original design, and those at the two transmission zeros are 0.7% and 1.1%. The measured results agree quite well with the simulations. It is evident that, without suffering from the need of extra circuit area, the proposed compact filtering antenna shown in Figure 3.16(a) has a flat passband radiation power as a function of frequency, high band-edge selectivity, and good stop-band suppression.

Table 3.1 Dimensions of the miniaturized coupled line resonator with unequal lengths in the compact filtering antenna I.

w_{a1}	l_{a1}	l_{a2}	l_{a3}	w_c	s_c
1.2	8.3	4.4	5.5	0.3	0.2

Unit: mm

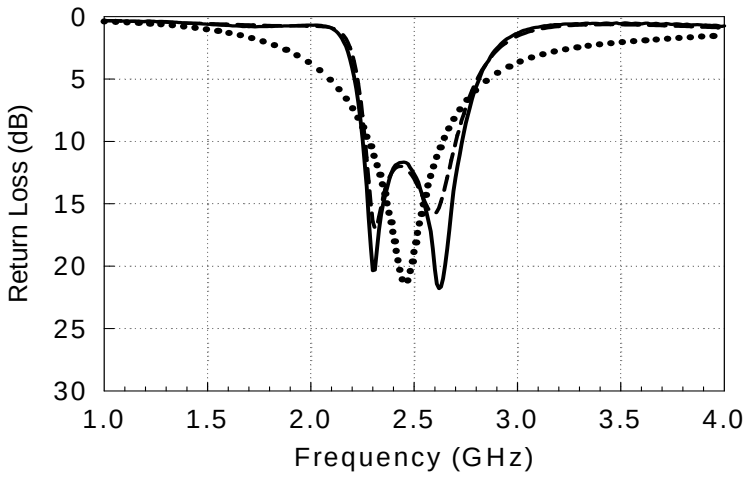

(a)

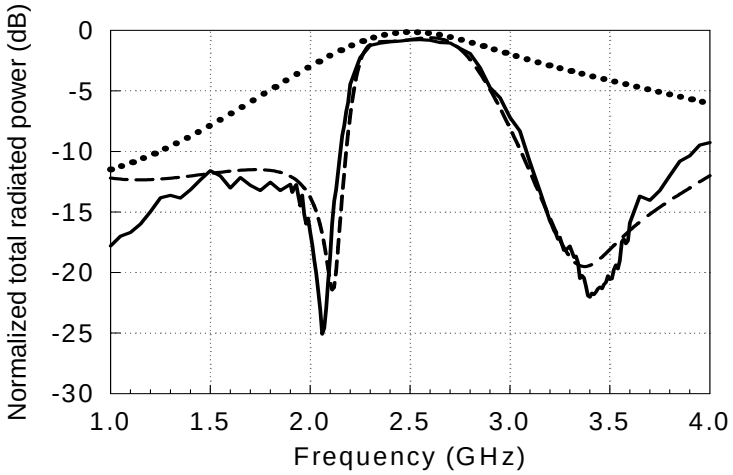

(b)

Figure 3.23 The simulated and measured results of the compact filtering antenna I in comparison with the simulated ones of the Γ-shaped antenna. (a) Return losses. (b) Normalized total radiated powers. [**—** : measurement of compact filtering antenna; ---- : simulation of compact filtering antenna; **….** : simulation of antenna only.]

Figure 3.24(a) and (b) show the full-wave simulated and measured antenna gains in the $+z$ and $+x$ directions versus frequency for the compact filtering antenna I. The simulated antenna gains of the Γ–shaped antenna in these two directions are also shown for reference. As expected, the antenna gains for the compact filtering antenna are flat in the passband. Also, two clear radiation nulls in the stop band can be observed in the simulation results, which make the band-edge selectivity and stop-band suppression better than those of the reference structure. The first null of the antenna gain locates at a frequency exactly equal to that (2.11 GHz) of the first null in the total radiation power response (Figure 3.23(b)). While the frequency location of the second null deviates a little from that in Figure 3.23(b) and depends on the observation angle, due to the influence of the antenna's radiation pattern. The measurement matches well to the simulation. The ripples in the stop band probably come from the non-ideal anechoic chamber condition. The measured antenna gains at f_0 = 2.45 GHz in the $+z$ and $+x$ directions, including the circuitry loss, are 1.03 dBi and -0.18 dBi, respectively.

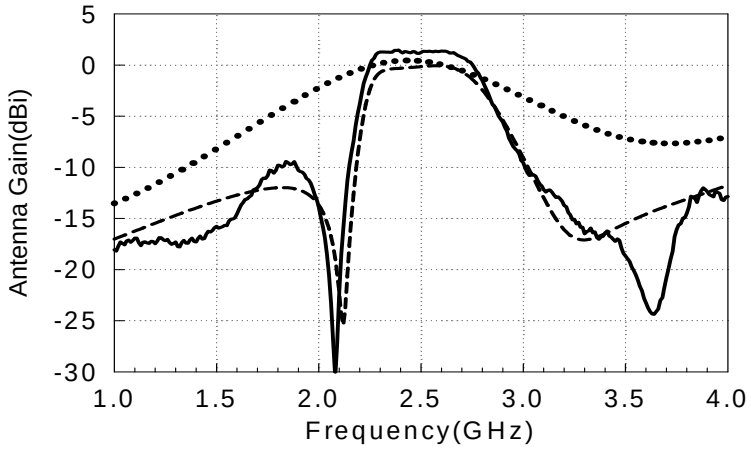

(a)

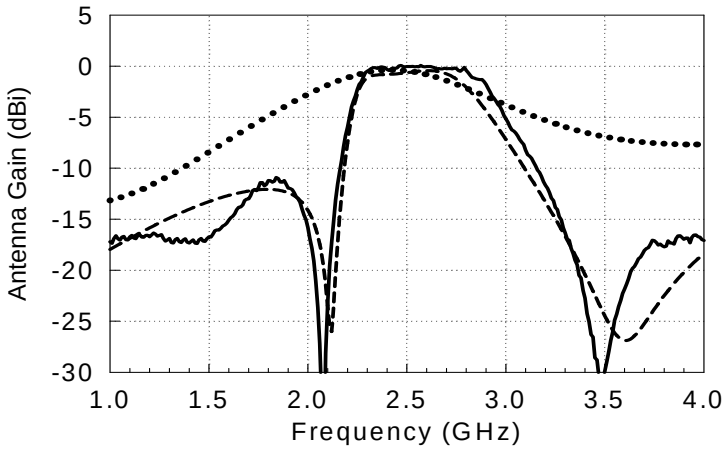

(b)

Figure 3.24 The simulated and measured antenna gains versus frequency of the compact filtering I antenna in comparison with the simulated ones of the Γ–shaped antenna. (a) In the +*z* direction and (b) in the +*x* direction. [— : measurement of compact filtering antenna; ---- : simulation of compact filtering antenna; **....** : simulation of antenna only.]

Figure 3.25 depicts the measured radiation patterns of the compact filtering antenna I at f_0 = 2.45 GHz in the three principal planes. The radiation pattern in the *xz*-plane is nearly omni-directional with peak gain of 1.2 dBi. Although not shown here, these patterns are about the same as the simulations and the measured results of the Γ–shaped antenna alone. Figure 3.26 shows the photograph of the finished compact filtering antenna.

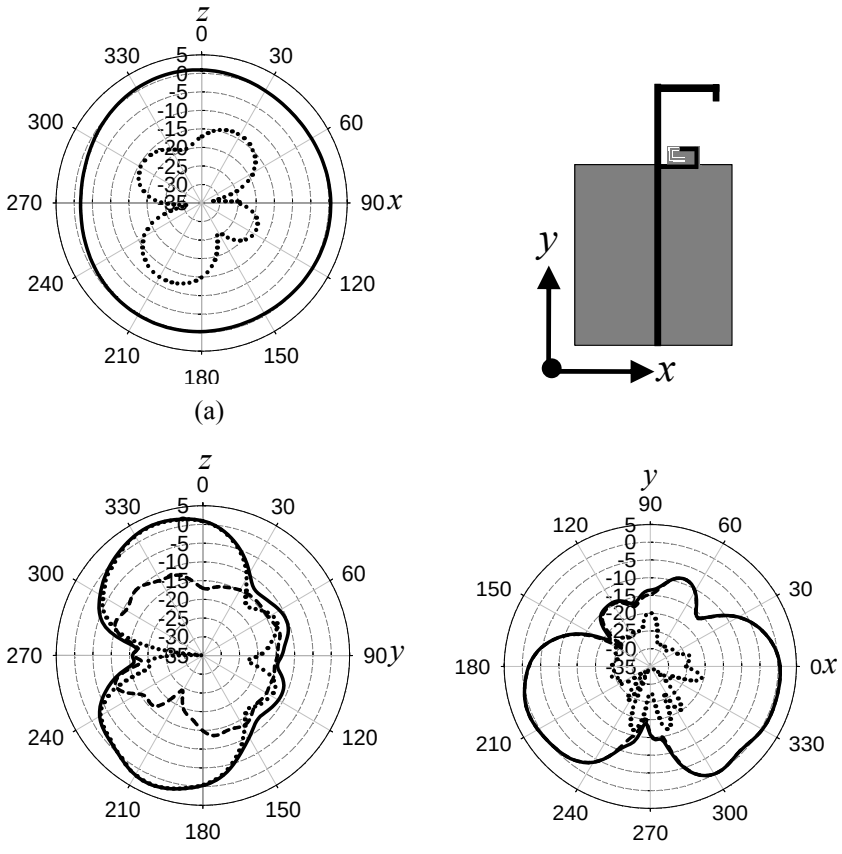

Figure 3.25 Measured radiation patterns of the compact filtering antenna I in the (a) xz-plane, (b) yz-plane, and (c) xy-plane. [— : E_{total}; --- : E_ϕ ; **....** : E_θ]. f_0 = 2.45 GHz.

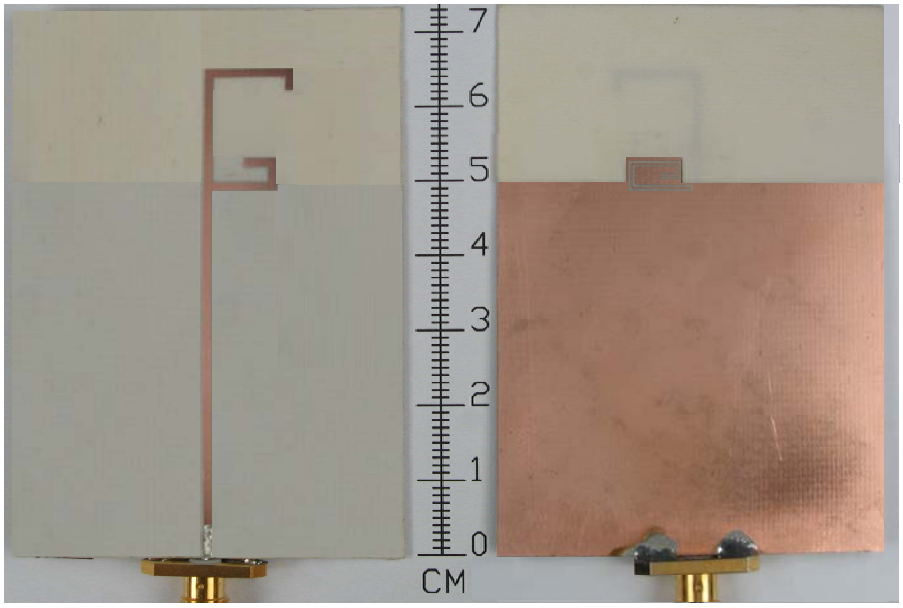

Figure 3.26 Photograph of the compact filtering antenna I. (left-side: top view; right-side: bottom view)

3.3.1 Compact Second-Order Filtering Antenna II

Following the design in Section 3.3.2, a new compact filtering antenna II, which consists of a miniaturized coupled line resonator and inverted-F antenna shown in Figure 3.27, is also proposed. Herein, an extended ground plane ($W_1 \times L_1$) is inserted between the vertical strips l_1 of the antenna. For the purpose of the more compact circuit size, a spiraled inverted-F antenna is also introduced [52].

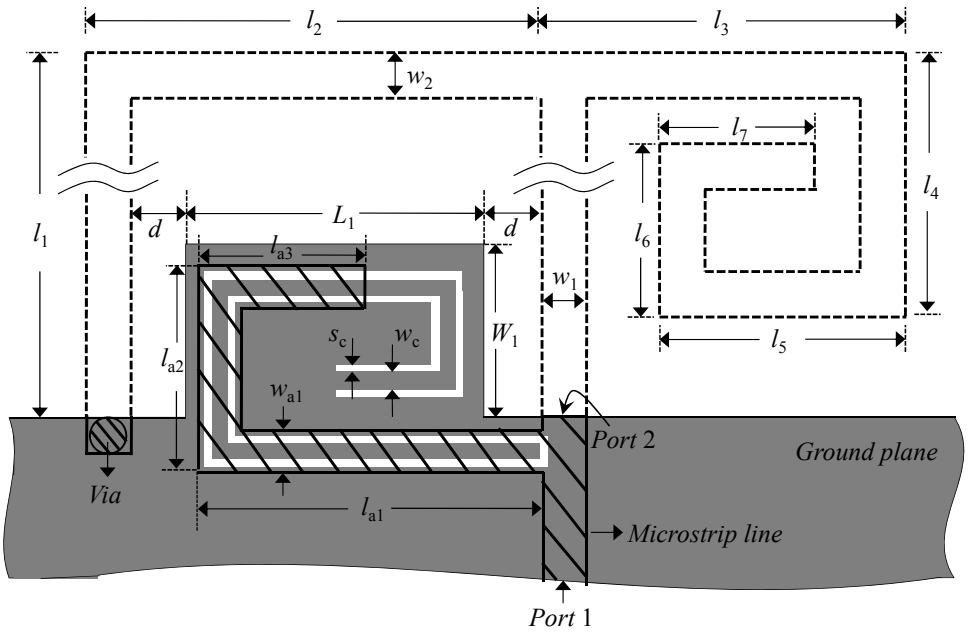

Figure 3.27 Geometry of the proposed miniaturized coupled line resonator in compact filtering antenna II.

As an example, a second-order Chebyshev bandpass filter with a 0.1 dB equal-ripple response, operating frequency f_0 = 2.45 GHz, a fractional bandwidth Δ = 10%, and Z_0 = 50 Ω is tackled. The filtering antenna is designed on a 0.8 mm thick FR4 substrate with a dielectric constant of 4.4 and loss tangent of 0.02. The

ground plane and the extended ground plane sizes are $L \times W$ = 50 mm×50 mm and $W_1 \times L_1$ = 5 mm × 50, respectively. According to the behaviors of the inverted-F antenna and the miniaturized coupled line resonator that depicted in Section 3.1.2 and Section 3.3.2, respectively, the suitable dimensions of the coupled line resonator can be designed based on the specifications of filter. The final dimensions of the compact filtering antenna II are listed in Table 3.2.

Table 3.2 Dimensions of the compact filtering antenna II.

l_1	l_2	l_3	l_4	l_5	l_6	l_7	l_{a1}
9	8	7	7	4.5	5	2.8	5.8
l_{a2}	l_{a3}	w_1	w_2	w_{a1}	w_c	s_c	d
6	2.6	1.53	1	1.2	0.5	0.2	1

Unit: mm

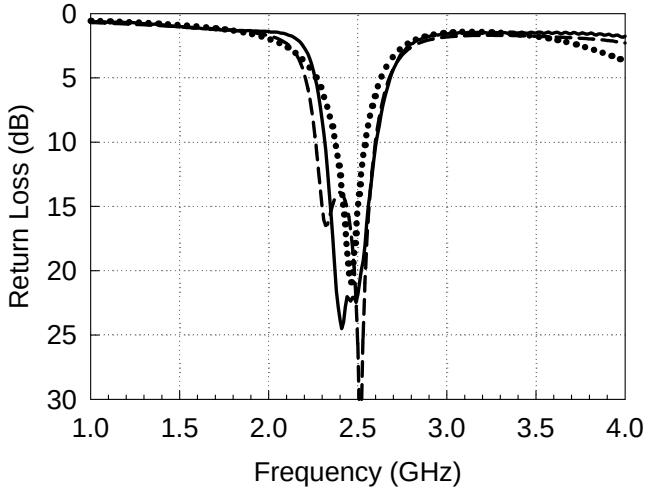

Figure 3.28 The simulated and measured return losses of the compact filtering antenna II in comparison with the simulated ones of the inverted-F antenna. [— : measurement of compact filtering antenna; ---- : simulation of compact filtering antenna; …. : simulation of antenna only.]

Figure 3.28 compares the simulated and measured return losses of the proposed filtering antenna. The simulated result of the spiraled inverted-F antenna is also shown for reference. Likely because of the deviations in dielectric constant and substrate thickness, the bandwidth of the measured return loss of the proposed filtering antenna is slightly narrower than the simulated one. The proposed filtering antenna exhibits a return loss larger than 15 dB over the passband, and provides better band-edge selectivity as compared the spiraled inverted-F antenna only.

Figure 3.29(a) shows the full-wave simulated and measured normalized total radiated powers of the compact filtering antenna. The simulated result of the spiraled inverted-F antenna is also shown for reference. It is seen that the full-wave simulated result of the compact filtering antenna shows two radiation nulls at 2.11 GHz and 3.12 GHz. The simulated radiation efficiency at operating frequency f_0 = 2.45 is about 70%, and those at the two transmission zeros are 1.1% and 1.6%. The lower radiation efficiency at operating

frequency may be caused by the loss tangent of the FR4 substrate. The measured results agree quite well with the simulations. It is evident that, without suffering from the need of extra circuit area, the proposed compact filtering antenna shown in Figure 3.16(b) has a good passband radiation power as a function of frequency, high band-edge selectivity, and better stop-band suppression.

Figure 3.29(b) shows the full-wave simulated and measured antenna gains in the +*z* direction versus frequency for the compact filtering antenna. The simulated antenna gains of the spiralled inverted-F antenna in the +z direction is also shown for reference. Two clear radiation nulls in the stop band can be observed in the simulation results, which make the band-edge selectivity and stop-band suppression better than that of the reference structure. The first null of the antenna gain locates at a frequency exactly equal to that (2.11 GHz) of the first null in the total radiation power response (Figure 3.29(a)). While the frequency location of the second null deviates a little from that in Figure 3.29(a) and depends on the observation angle, due to the influence of the antenna's radiation pattern. The measurement matches well to the simulation. The ripples in the stop band probably come from the non-ideal anechoic chamber condition. The measured antenna gain at f_0 = 2.45 GHz in the +*z* directions, including the circuitry loss, is -1.01 dBi.

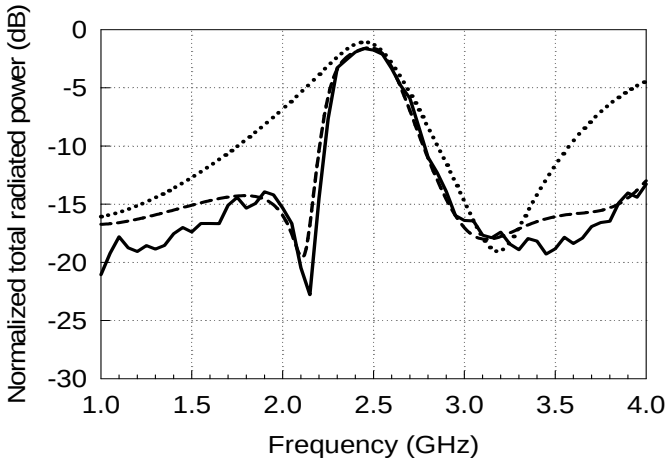

(a)

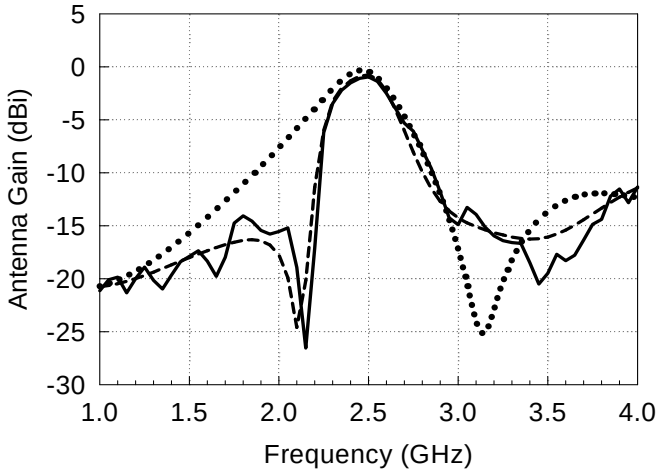

(b)

Figure 3.29 The simulated and measured results of the compact filtering antenna II in comparison with the simulated ones of the inverted-F antenna. (a) total radiated powers and (b) antenna gains in the +z direction. [**—** : measurement of compact filtering antenna; **----** : simulation of compact filtering antenna; **….** : simulation of antenna only.]

Figure 3.30 depicts the measured radiation patterns of the compact filtering antenna at f_0 = 2.45 GHz in the three principal planes. The radiation pattern in the *xz*-plane is nearly omni-directional with peak gain of 0.34 dBi. Although not shown here, these patterns are about the same as the simulations and the measured results of the spiraled inverted-F antenna alone. Figure 3.31 shows the photograph of the finished compact filtering antenna.

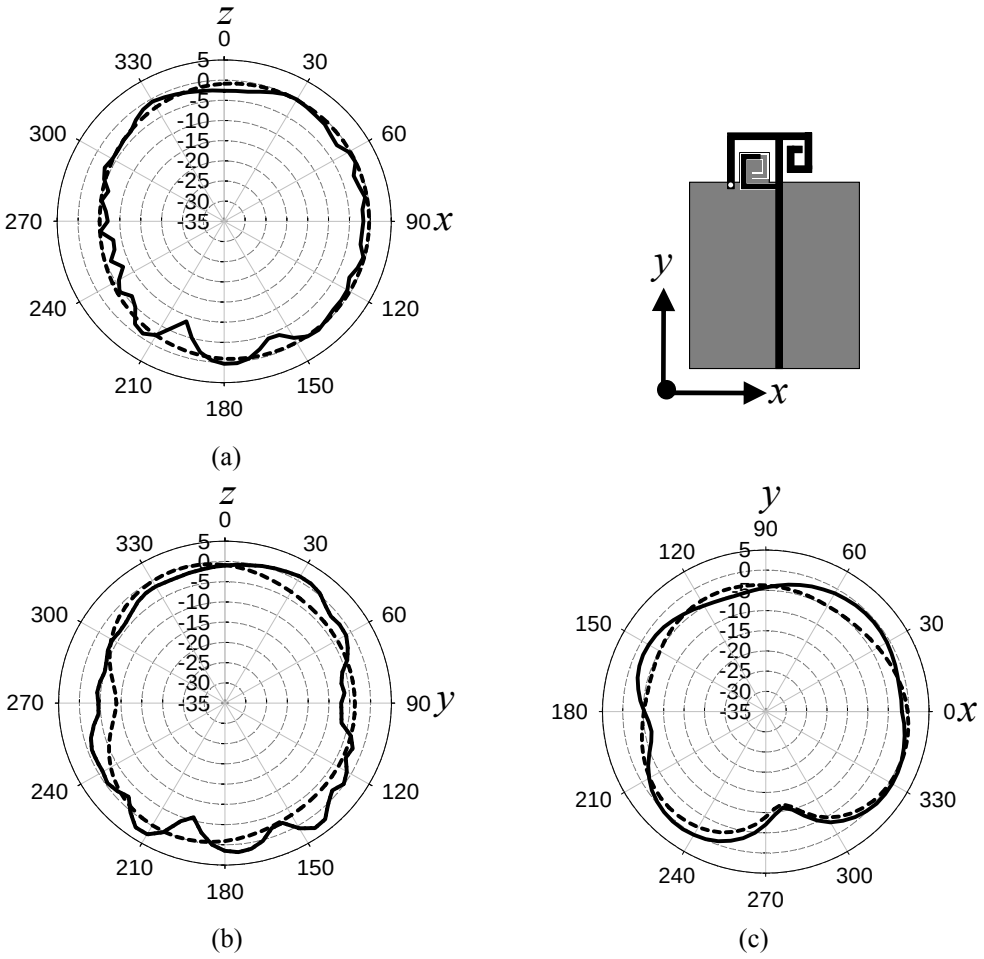

Figure 3.30 Measured and simulated total-field radiation patterns in the (a) *xz*, (b) *yz*, and (c) *xy* planes for the compact filtering antenna II. [solid line: measured results; dashed line: full-wave simulated results]. f_0 = 2.45 GHz.

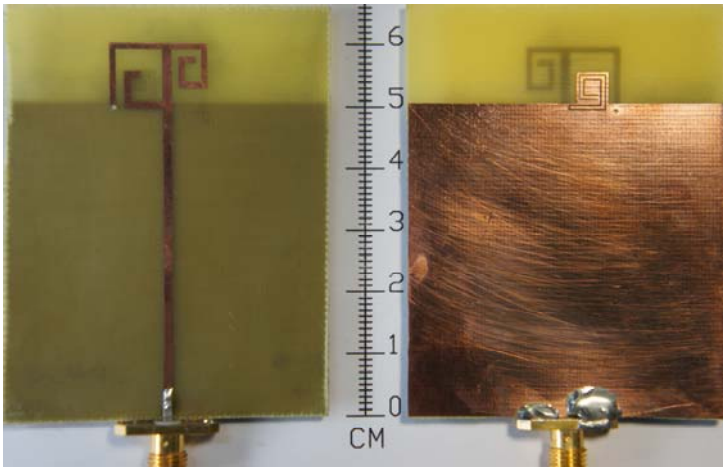

Figure 3.31 Photograph of the compact filtering antenna II. (left-side: top view; right-side: bottom view)

3.4 Summary

A filtering antenna with new co-design approach has been proposed and implemented. The design is accomplished by first extracting the circuit model of the antenna, then casting it into the synthesis of a typical parallel coupled line filter. To increase the fabrication tolerance, a quarter-wave admittance inverter with characteristic impedance other than Z_0 is introduced in the filter synthesis. A design example which has the same specifications as the conventional third-order Chebyshev bandpass filter is demonstrated. The proposed filtering antenna provides good skirt selectivity as the conventional bandpass filter. In addition, the novel printed filtering antennas with very compact configurations also have been demonstrated. By incorporating a ground-intruded miniaturized coupled line resonator, the proposed filtering antennas occupied about the same substrate area as the conventional printed antennas, while exhibited flat high band-edge selectivity, and good stop-band suppression. Thorough analysis and design of the coupled line resonator and the filtering antenna have been described. The measured results, including the return loss, total radiation power, and antenna gains versus frequency, agree quite well with the simulated ones. It also possesses flat antenna gain in the passband and high suppression in the stopband.

Chapter 4 Band-Notched UWB Monopole Antenna

This chapter presents a novel design of band-notched ultra-wide-band (UWB) monopole antenna with high notch-band-edge selectivity. The proposed antenna consists of a radiation patch and an embedded second-order bandstop filter. Using the same substrate area as a fundamental UWB antenna, a bandstop filter composed of a non-uniform short-circuited stub and coupled open-/short-circuited stub resonators, is designed into the fundamental antenna. A detail design procedure for the proposed antenna with a second-order Maxially-flat bandstop filter at 5.5 GHz is presented. As compared to the fundamental antenna, the proposed UWB antenna provides good notch-band suppression from 5.15 GHz to 5.95 GHz in which the normalized total radiated powers in the notch-band are lower than -12 dB. Also, the proposed structure provides high band-edge selectivity and flat return loss in the notch-band. The measured results, including the return loss, total radiated power, agree with the designed ones.

4.1 Antenna Configuration and Equivalent Circuit

Figure 4.1(a) shows the geometry of the proposed UWB antenna, which is a three-layer structure with two FR4 substrates in between. Each substrate has a thickness of 0.4 mm, dielectric constant of 4.4, and loss tangent of 0.02. Figure 4.1(b), (c), and (d) depict, respectively, the top view, middle view, and bottom view of antenna layout. A signal is to be fed from a 50 Ω microstrip feed line with signal line on the top layer and ground on the bottom layer. The signal line is connected to a trapezoid patch (with dimensions of w_{b1}, w_{b2}, l_b) at point A as shown in Figure 4.1(b). The trapezoid patch is then connected to a pentagon patch on the middle layer through a row of vias (heavy dots in Figure 4.1(b) and (c)). Here, the pentagon patch (with dimensions of l_a, w_a, l_s, w_s), together with the ground plane on the bottom layer, is the main UWB radiator. Apparently, these two metal patches form a non-uniform short-circuited stub when looking upwards at the port between points A and C (Figure 4.1(c)). The length l_b of the stub is about a quarter guided wavelength at the center frequency of the notch band. On the bottom layer, two closely spaced strips of different lengths are joined to the ground plane at point B as shown in Figure 4.1(d). The shorter strip is connected to the radiation patch on the middle layer through a via. Therefore, when looking upwards at the port between points C and B, one sees a coupled short-circuited stub and open-circuited stub in shunt. The lengths of these two stubs are both near to a quarter guided wavelength at the notch band. Note that the pentagon patch not only behaves as a radiator but also the ground plane of these stub resonators. The whole antenna size $W \times L$ measures 30 mm × 27.6 mm, including the ground plane size $W \times l_g$ of 30 mm × 10 mm.

Figure 4.2 illustrates the equivalent circuit of the proposed antenna around the notch band. To realize this circuit, let us start from the feed point A of the antenna. Since the non-uniform short-circuited stub is a quarter-wavelength long, a shunt LC resonator (L_1, C_1) with resonant frequency at 5.5 GHz appears in between points A and C. Between point C and ground point B, two circuit components are connected in parallel. The first is the coupled stub resonator, which functions as a series LC resonator (L_2, C_2), mainly due to the open-circuited stub. And the second is the UWB antenna, formed by the pentagon patch on the middle layer and the ground plane on the bottom layer. Here, since the antenna is to be designed with good

performance covering the whole ultra wide band, it is thus modeled as a radiation resistance R_A (about 50 Ω) around the notch band [29].

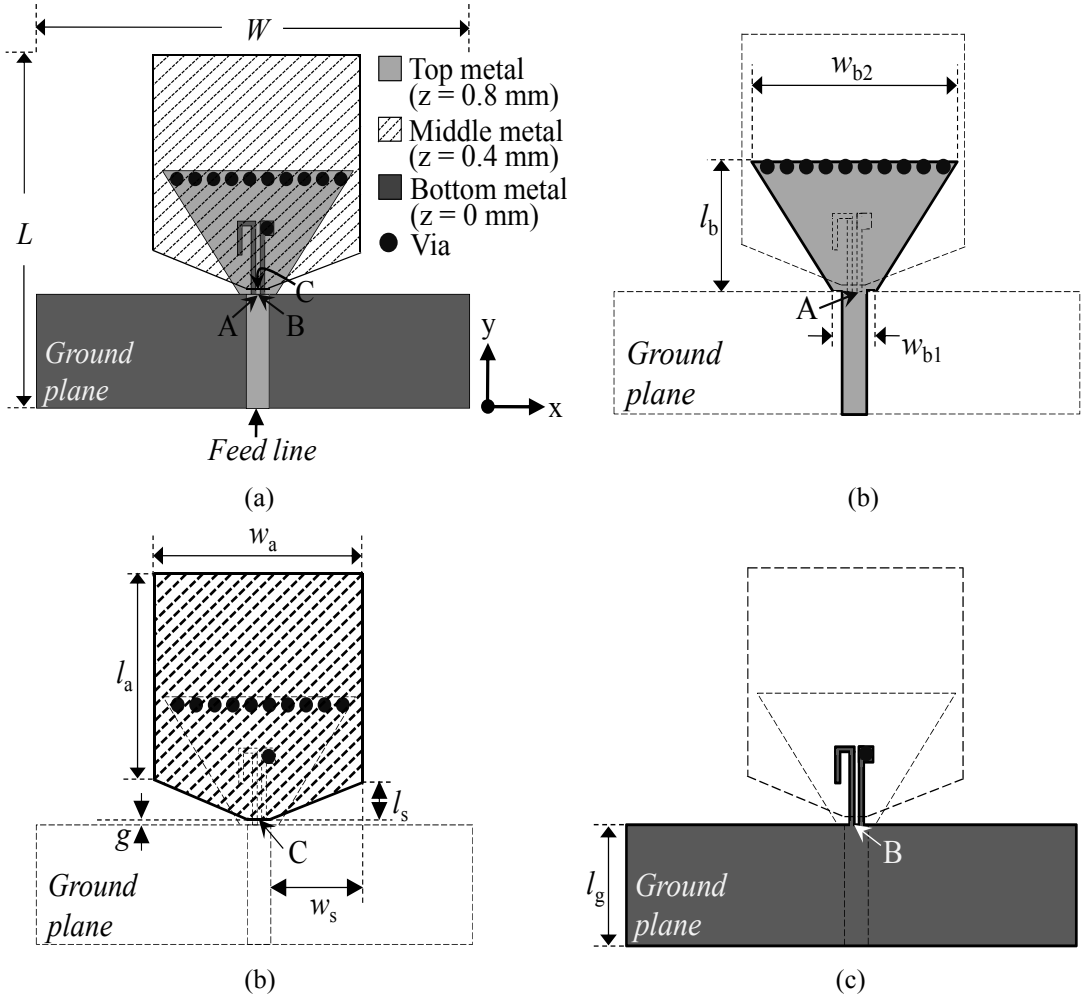

Figure 4.1 Geometry of the proposed band-notched UWB monopole antenna. (a) Perspective-view. (b) Top-view. (c) Middle-view. (d)Bottom-view.

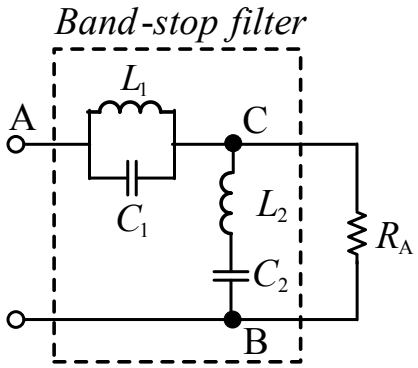

Figure 4.2 Equivalent circuit of the proposed band-notched UWB monopole antenna.

From the equivalent circuit in Figure 4.2, it is obvious that the proposed structure has the function of, not only an UWB antenna, but also a second-order bandstop filter. When a signal of frequency in the notch band enters the structure, it will be reflected back due to the presence of the stub resonators; while as the signal is of other frequency, it will be successfully delivered to the radiation patch and radiated out.

4.2 Antenna Design

In this section, the design of the fundamental UWB monopole antenna covering the full UWB band (3.1-10.6 GHz) is first introduced. And then, the non-uniform short-circuited stub resonator is tackled. By using the coupled open-/short-circuited stub resonator that discussed in Chapter 2.2, a second-order bandstop filter can be realized. Finally, the synthesis of the proposed band-notched UWB monopole antenna is summarized.

A. Fundamental UWB Antenn

Various radiation patch shapes of the planar monopole antennas have been studied and utilized to attain the UWB properties. Figure 4.3(a) shows the fundamental UWB monopole antenna used in this study. The radiation patch is connected to the 50 Ω microstrip line on the top side of the FR4 substrate with thickness of 0.4 mm. The pentagonal shape of the radiator is obtained by trimming the lower edge of a square patch so as to enhance the upper bandwidth. Since a monopole-like UWB antenna at higher frequency usually behaves as a slot antenna [31], properly designing the shape of the bevels on the lower side will certainly improve the excitation of the slot-mode radiation. On the other hand, the current at low frequency is mainly distributed over the patch and the ground plane, which is similar to that of a printed finite-ground monopole antenna. For a given ground plane length (l_g), the patch length, l_a, will determine the lowest operation frequency. The gap, g, between the pentagon patch and the ground plane is also an important parameter, which will influence the impedance matching of the antenna. The final design of the fundamental UWB antenna measures the following structure dimensions: $w_a \times l_a$ = 14 mm × 15.7 mm, $w_s \times l_s$ = 6.24 mm × 1.4 mm, g = 0.5 mm, and $W \times l_g$ = 30 mm × 10 mm. Figure 4.3(b) shows the simulated input impedance by using the full-wave simulation solver HFSS [51]. As expected, the real part of the impedance is near 50 Ω and the imaginary part almost zero, especially in the range from 4 GHz to 7.5 GHz. The input impedance of the antenna can be further improved over a wider frequency range by properly shaping the ground plane edge.

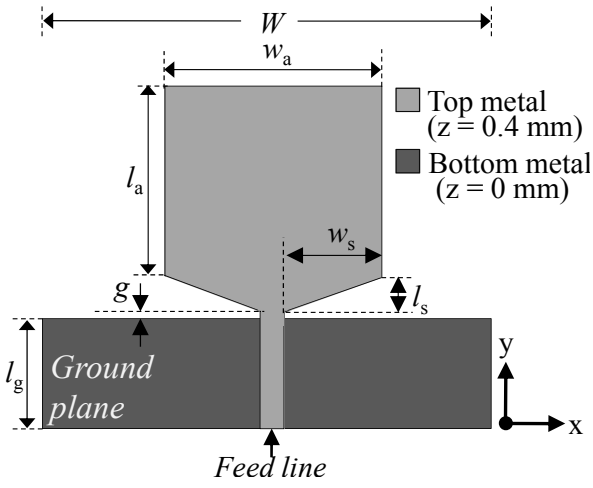

(a)

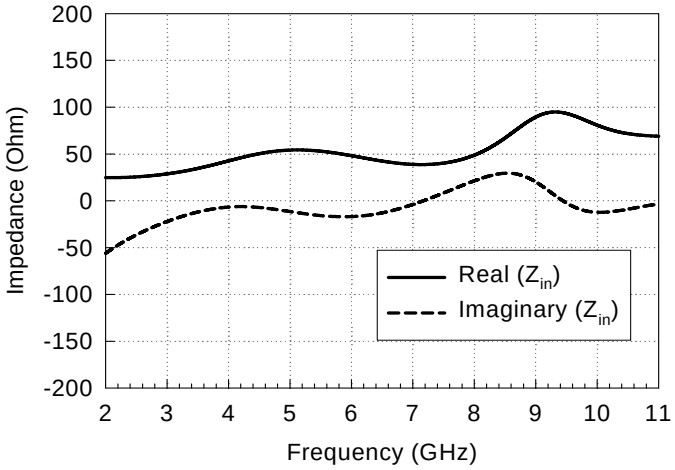

(b)

Figure 4.3 Fundamental UWB antenna. (a) Configuration. (b) Full-wave simulated input impedance.

B. Non-uniform Short-Circuited Stub Resonator

To design a shunt *LC* resonator with narrow bandwidth, a high capacitance is needed. Generally, a high-capacitance *LC* resonator can be implemented by using a wide λ/4 short-circuited microstrip stub. However, the large strip width of the resonator may cause transverse resonance, thus destroying the resonator function. The intrusion of the wide strip into the slot region between the radiation patch and the ground plane may also deteriorate the slot-mode radiation of the antenna. To avoid these problems, here a non-uniform λ/4 short-circuited microstrip stub, as shown in Figure 4.1(b), is utilized. Figure 4.4 shows the extracted capacitance C_1 of this non-uniform stub by using the circuit simulation tool AWR [48]. By keeping a small strip width (w_{b1} = 2.5 mm) so as not to destroy the radiation slot mode, a λ/4 short-circuited stub resonator with sufficient capacitance can be obtained by choosing a suitable strip width (w_{b2}) at the short-circuited end.

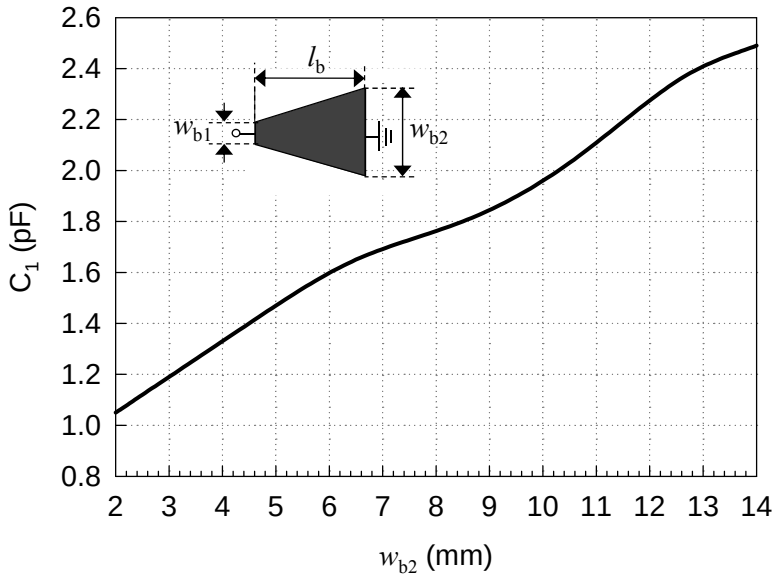

Figure 4.4 The extracted capacitances C_1 of the non-uniform short-circuited microstrip stub resonators as a function of the strip width w_{b2}. (w_{b1} = 2.5 mm and l_b = 90° at f_0= 5.5 GHz)

C. Synthesis of the Antenna

After designing all the required components as above and the coupled open-/short-circuited stub resonator in Section 2.2, one may now integrate them together to synthesize the band-notched UWB antenna by using the following steps:

1) Suitably design the fundamental UWB antenna as shown in Figure 4.3(a) with the bandwidth covering from 3.1 to 10.6 GHz.
2) Specify the requirements of the bandstop filter to be synthesized, including the operating frequency f_0, the fractional bandwidth Δ, and the type of the filter (e.g., bandstop filter with maximally flat response), from which the circuit elements (L_1, C_1, L_2, C_2) of a typical bandstop filter in Figure 4.2 can be obtained by using the following equations [47]:

$$L_1 = \frac{Z_0 g_1 \Delta}{2\pi f_0} \tag{4.1}$$

$$L_2 = \frac{Z_0}{2\pi f_0 g_2 \Delta} \tag{4.2}$$

where $f_0 = \frac{1}{2\pi\sqrt{L_1 C_1}} = \frac{1}{2\pi\sqrt{L_2 C_2}}$, and g_1, g_2 are the component values of the low-pass prototype filter [47].

3) Using the component values of C_1 and L_2 obtained above; determine the dimensions of the non-uniform short-circuited stub and the coupled stub resonators with equal stub length according to Figure 4.4 and Figure 2.6, respectively.
4) Properly shorten the short-circuited stub's length (θ_{c1}) in the coupled stub resonator (as shown Figure 2.5(c)) so as to adjust the positions of the transmission poles until the bandwidth of the whole UWB antenna is enough.

4.3 Experimental Results

Following the above design procedures, the fundamental UWB monopole antenna is first designed with dimensions of $w_a \times l_a$ = 14 mm × 15.7 mm, $w_s \times l_s$ = 6.24 mm × 1.4 mm, and g = 0.5 mm. Secondly, based on the requirement of band notch from 5.0 GHz to 6.0 GHz, the embedded bandstop filter is specified as one with maximally flat response, center frequency f_0 = 5.5 GHz, fractional bandwidth Δ= 18%, and Z_0 =50. Thus, the circuit components of the filter can be calculated, using (1) and (2), as L_1 = 0.37 nH, C_1 = 2 .27 pF, L_2 = 5.68 nH, and C_2 = 0.15 pF. Then, with the value of C_1 and from Figure 5.4, the dimensions of the non-uniform short-circuited stub can be decided, which are w_{b1} = 2.5 mm, w_{b2} = 12 mm, and l_b =8.6 mm. Also, by using the calculated component L_2 and Figure 2.6, the line width and gap size of the λ/4 coupled open-/short-circuited stub resonator with equal length can be obtained, which are 0.12mm, 0.12mm, respectively. To this step, one now assembles all the components according Figure 4.1 to form the

band-notched UWB antenna. Finally, to achieve the required antenna bandwidth, the electric length θ_{c1} of the short-circuited stub is shorten from 90° to 50° by full-wave simulation for the whole structure.

Figure 4.5(a) shows the full-wave simulated and measured return losses of the designed UWB antenna. The simulated result of the fundamental UWB antenna without band notch is also shown for reference. The measured return loss of the proposed UWB antenna is in close agreement with the simulated one. It is obvious that the low frequency band of the proposed UWB antenna is wider than the one of the fundamental UWB antenna due to the existence of the transmission pole at low frequency generated by the coupled stub resonator. Apparently, the embedded bandstop filter in the proposed antenna successfully blocks the input signal from 5 GHz to 6 GHz to radiate. The return loss in this frequency range is quite flat with a value of about 2.5 GHz. Outside this notch band, it rapidly increases to be larger than 10 dB. Good band-edge selectivity is achieved. Note that the non-zero dB return loss in the notch band is due to the substrate and metal losses produced in the filter resonators.

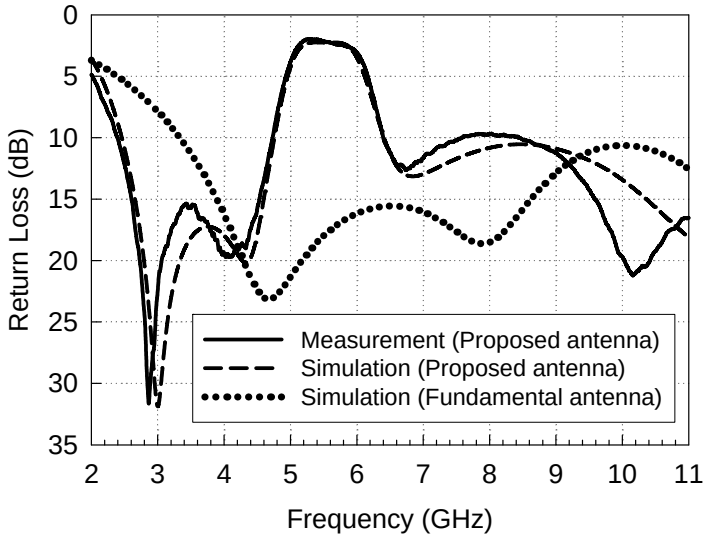

(a)

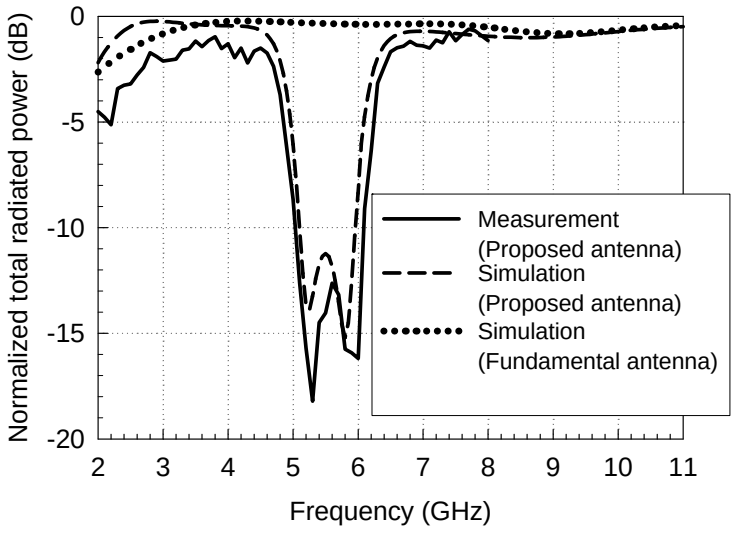

(b)

Figure 4.5 Simulated and measured results of the proposed UWB monopole antenna in comparison with the simulated ones of the fundamental UWB antenna. (a) Return losses. (b) Normalized total radiated powers.

Figure 4.5(b) shows the full-wave simulated and measured total radiated powers of the proposed band-notched UWB antenna, together with simulated one of the fundamental UWB antenna. Here, the total radiated power has been normalized to the input power, which is thus equal to the efficiency of the antenna. Note that the total radiated power is measured only from 2 to 8 GHz due to the limited frequency range of the available 3D RF anechoic chamber. It is seen that the simulated result of the proposed UWB antenna has two radiation nulls at 5.25 GHz and 5.8 GHz. As compared to the fundamental UWB antenna, the proposed antenna provides good notch-band suppression from 5 GHz to 6 GHz in which the normalized total radiated power is lower than -10 dB. Also, the proposed structure possesses high notch-band-edge selectivity. The simulated radiation efficiency of the proposed UWB antenna at the frequency of 5.5 GHz is only 7.5% and at the two radiation nulls are less than 5%. While outside the notch band, the proposed antenna has about the same total radiation power (or antenna efficiency) as the fundamental UWB antenna. The measured result of the proposed structure agrees quite well with the simulated one.

Figure 4.6 illustrates the simulated current distributions at 4 GHz, 5.5 GHz, and 8 GHz for the proposed antenna structure. It is seen that at frequencies (4 GHz and 8 GHz) in the passband, many currents are distributed around the radiation patch and the ground plane, which contribute to the radiation of the antenna. The current distribution at the low frequency (4 GHz) is standing-wave type, like that of a monopole antenna, and that at the high frequency (8 GHz) is traveling-wave type, corresponding to a tapered slot antenna. On the contrary, the current at the notch frequency (5.5 GHz) is mainly concentrated on the non-uniform short-circuited stub and the coupled stub resonator. The current on the radiation patch and the ground plane is much weaker, thus resulting in a negligible radiation field as compared to those at frequencies in the passband.

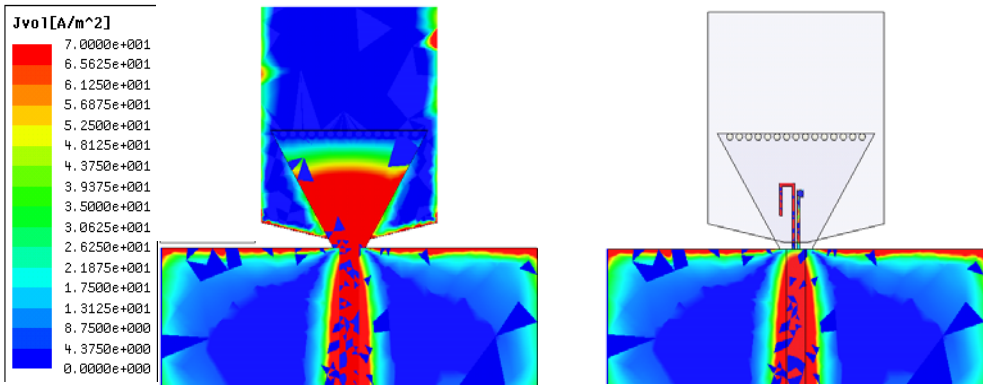

(a)

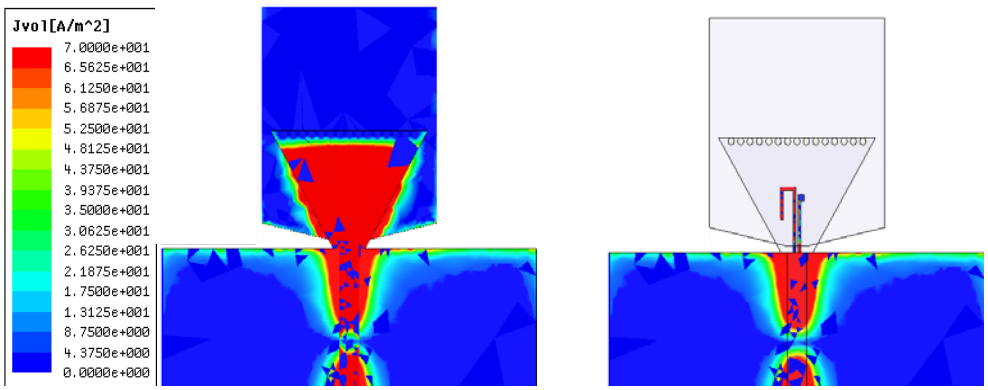

(b)

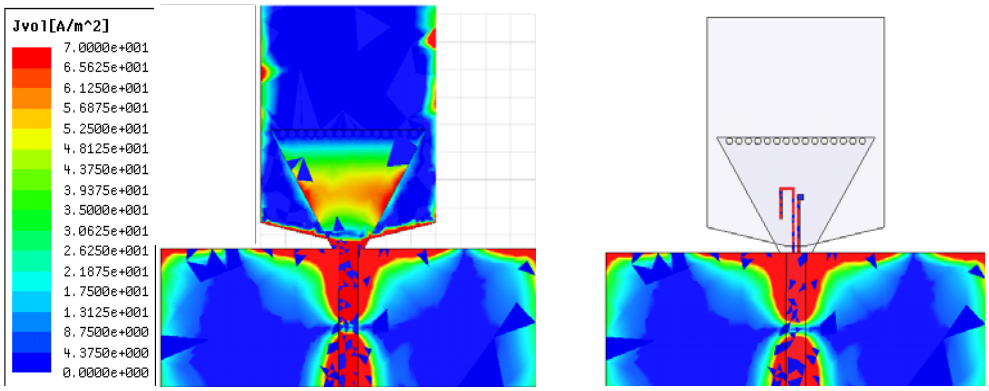

(c)

Figure 4.6 Simulated current distributions of the proposed UWB monopole antenna at (a) f = 4 GHz, (b) f = 5.5 GHz, and (c) f = 8 GHz.

The measured total-field radiation patterns of the proposed UWB antenna at the low, notch, and high frequency bands in the *xz*-plane are depicted respectively in Figure 4.7(a), (b), and (c). All the radiation patterns are quite omni-directional. The antenna gains at the low and high frequency bands are about 0 dBi, while those at the notch band are below -10 dBi. Figure 4.8 shows the photograph of the fabricated band-notched UWB antenna.

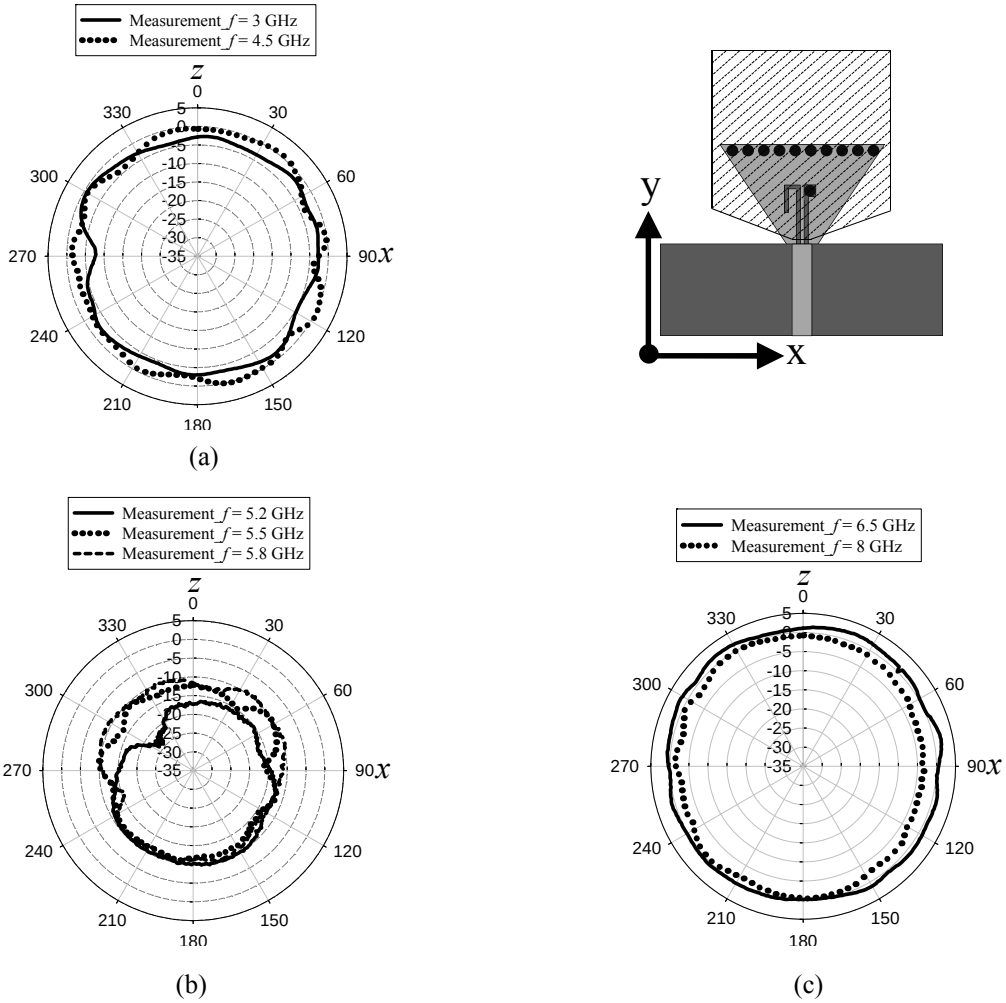

Figure 4.7 Measured total-field radiation patterns of the proposed UWB antenna at (a) low, (b) notch, and (c) high frequency bands in the xz-plane. (Unit: dBi)

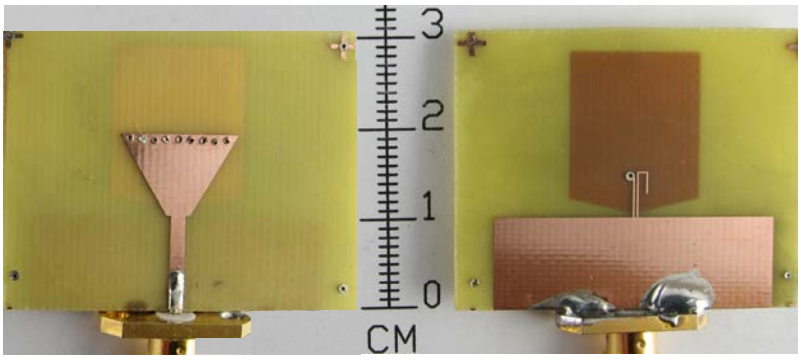

Figure 4.8 Photograph of the proposed UWB antenna. (left-side: top view; right-side: bottom view)

4.4 Summary

A new UWB monopole antenna with band-notched characteristic in the frequency range from 5 GHz to 6 GHz has been proposed and demonstrated. Occupying about the same substrate area as a conventional UWB antenna, a second-order bandstop filter, realized by a non-uniform short-circuited stub and an open-/short-circuited stub resonator, has been designed to merge into the UWB antenna. The measured 10-dB return loss bandwidth covered the range from 2.4 GHz to over 11 GHz with a 3-dB notched band from 5.0 GHz to 6.0 GHz. Good notch-band rejection and notch-band-edge selectivity were achieved. Also, the measured radiation patterns of the proposed antenna in the H plane are omni-directional, with antenna gains about 0 dBi at frequencies in the passband and below -10 dBi at notch frequencies. Finally, the measured results, including the return loss and total radiated power, showed good agreement with the design ones.

Chapter 5 Conclusions

Several compact filtering antennas with good frequency responses as a filter, have been demonstrated successfully in this project. The conclusions for whole researches are listed below.

Chapter 2 mainly discusses the novel coupled line resonator and coupled open-/short-circuited stub resonator. Without using the cross-coupling mechanism, the proposed coupled line resonator has provided not only a transmission pole near the center frequency but one pair of tunable transmission zeros at the two sides. In addition, the coupled open-/short-circuited stub resonator has displayed a transmission zero at the center frequency and one pair of tunable transmission poles at the two sides. Compared to the conventional stub resonator, the proposed coupled one produces higher inductance near the center frequency, which can be used to design a narrow-bandwide bandstop filter. Occupying the small circuit size, both the proposed coupled resonators can provide high band-edge selectivity.

In Chapter 3, the new printed filtering antennas using the co-design approach to synthesize, have been proposed and implemented. The designs are accomplished by first extracting the circuit model of the antennas, then casting it into the synthesis of a typical parallel coupled line filter. A filtering antenna which contains an inverted-L antenna and parallel half-wavelength microstrip line resonators, has been first demonstrated. Furthermore, the new printed filtering antennas with very compact configuration have been demonstrated. By incorporating a ground-intruded miniaturized coupled line resonator, the proposed filtering antenna occupied about the same substrate area as a conventional printed antenna, while exhibited flat high band-edge while exhibited flat high band-edge selectivity, and good stop-band suppression. Thorough analysis and design of the coupled line resonator and the filtering antenna have been described. The measured results, including the return loss, total radiation power, and antenna gains versus frequency, have good agreement with the design ones.

Finally, in Chapter 4, a new UWB monopole antenna with band-notched characteristic in the frequency range from 5 GHz to 6 GHz has been proposed and demonstrated. Occupying about the same substrate area as a conventional UWB antenna, a second-order bandstop filter, realized by a non-uniform short-circuited stub and an open-/short-circuited stub resonator, has been designed to merge into the UWB antenna. Good notch-band rejection and notch-band-edge selectivity were achieved. Also, the measured radiation patterns of the proposed antenna in the H plane are omni-directional, with antenna gains about 0 dBi at frequencies in the passband and below -10 dBi at notch frequencies. Finally, the measured results, including the return loss and total radiated power, showed good agreement with the design ones.

References

[1] H. An, B. K. J. C. Nauwelaers, and A. R. V. D. Capelle, "Broadband microstrip antenna design with the simplified real frequency technique," *IEEE Trans. Antennas Propag.*, vol. 42, pp. 129–135, Feb. 1994.

[2] B. Froppier, Y. Mahe, E. M. Cruz, and S. Toutain, "Integration of a filtering function in an electromagnetic horn," in *Proc. 33th Eur. Microw. Conf.*, 2003, pp. 939-942.

[3] F. Queudet, B. Froppier, Y. Mahe, and S. Toutain, "Study of a leaky waveguide for the design of filtering antennas," in *Proc. 33th Eur. Microw. Conf.*, 2003, pp. 943-946.

[4] G. Q. Luo, W. Hong, H. J. Tang, J. X. Chen, X. X. Yin, Z. Q. Kuai, and K. Wu, "Filtenna consisting of horn antenna and substrate integrated waveguide cavity FSS," *IEEE Trans. Antennas Propag.*, vol. 55, no. 1, pp. 92-98, Jan. 2007.

[5] F. Queudet, I. Pele, B. Froppier, Y. Mahe, and S. Toutain, "Integration of pass-band filters in patch antennas," in *Proc. 32th Eur. Microw. Conf.*, 2002, pp. 685-688.

[6] W.-G. Yeo, T.-Y. Seo, J. W. Lee, and C. S. Cho, "H-plane sectoral filtering horn antenna in PCB substrates using via fences at millmeter-wave," in *Proc. 37th Eur. Microw. Conf.*, 2007, pp. 818-821.

[7] J.-H. Lee, N. Kidera, S. Pinel, J. Laskar, and M. M. Tentzeris, "Fully integrated passive front-end solutions for a V-band LTCC wireless system," *Antennas Wireless Propag. Lett.*, vol. 6, pp. 285-288, 2007.

[8] N. Yang, C. Caloz, and K. Wu, " Co-designed CPS UWB filter-antenna system," in *Proc. IEEE AP-S Int. Symp.*, Jun. 2007, pp. 1433-1436.

[9] C.-H. Wu, C.-H. Wang, S.-Y. Chen, and C. H. Chen, "Balanced-to-unbalanced bandpass filters and the antenna applications," *IEEE Trans. Microw. Theory Tech.*, vol. 56, no. 11, pp. 2474-2482, Nov. 2008.

[10] M. Troubat, S. Bila, M. Thevenot, D. Baillargeat, T. Monediere, S. Verdeyme, and B. Jecko, "Mutual synthesis of combined microwave circuits applied to the design of a filter-antenna subsystem," *IEEE Trans. Microw. Theory Tech.*, vol. 55, no. 6, pp. 1182-1189, Jun. 2007.

[11] H. Blondeaux, D. Baillargeat, P. Leveque, S. Verdeyme, P. Vaudon, P. Guillon, A. Carlier, and Y. Cailloce, "Microwave device combining and radiating functions for telecommunication satellites," in *IEEE MTT-S Int. Microw. Symp. Dig.*, May 2001, pp. 137-140.

[12] T. L. Nadan, J. P. Coupez, S. Toutain, and C. Person, "Optimization and miniaturization of a filter/antenna multi-function module using a composite ceramic-foam substrate," in *IEEE MTT-S Int. Microw. Symp. Dig.*, Jun. 1999, pp. 219-222.

[13] S. Oda, S. Sakaguchi, H. Kanaya, R. K. Pokharel, and K. Yoshida, "Electrically small superconducting antennas with bandpass filters," *IEEE Trans. Appl. Supercond.*, vol. 17, no. 2, pp. 878-881, Jun. 2007.

[14] A. Abbaspour-Tamijani, J. Rizk, and G. Rebeiz, " Integration of filters and microstrip antennas," in *Proc. IEEE AP-S Int. Symp.*, Jun. 2002, pp. 874-877.

[15] L.-H. Hsieh and K. Chang, "Tunable microstrip bandpass filters with two transmission zeros," *IEEE Trans. Microw. Theory Tech.*, vol. 51, no.2, pp. 520-525, Feb. 2003.

[16] L. Zhu and W. Menzel, “Compact microstrip bandpass filter with two transmission zeros using a stub-tapped half-wavelength line resonator,” *IEEE Microw. Wireless Compon. Lett.*, vol. 13, no. 1, pp. 16-18, Jan. 2003.

[17] K.-S. Chin, Y.-C. Chiang, and J.-T. Kuo, “Microstrip open-loop resonator with multispurious suppression,” *IEEE Microw. Wireless Compon. Lett.*, vol. 17, no. 8, pp. 574-576, Aug. 2007.

[18] C.-L. Hsu and J.-T. Kuo, “Design of cross-coupled quarter-wave SIR filters with plural transmission zeros,” in *IEEE MTT-S Int, Microwave Symp*. Dig., San Francisco, 2006, pp. 1205-1208.

[19] C.-H. Wu, Y.-S. Lin, C.-H. Wang, and C. H. Chen, “Compact microstrip coupled-line bandpass filter with four transmission zeros,” *IEEE Microw. Wireless Compon. Lett*., vol. 15, no. 9, pp. 579-581, Sep. 2005.

[20] C. Y. Chang and C. C. Chen, “A novel coupling structure suitable for cross-coupled filters with folded quarter-wave resonators,” *IEEE Microw. Wireless Compon. Lett*., vol. 13, no. 12, pp. 517-519, Dec. 2003.

[21] C. K. Liao and C. Y. Chang, “Modified parallel-coupled filter with two independently controllable upper stopband transmission zeros,” *IEEE Microw. Wireless Compon. Lett*., vol. 15, no. 12, pp. 841-843, Dec.2005.

[22] C. K. Liao and C. Y. Chang, “Design of microstrip quadruplet filters with source-load coupling,” *IEEE Trans. Microw. Theory Tech*., vol. 53, no.7, pp. 2302-2308, Jul. 2005.

[23] P.-H. Deng, Y.-S. Lin, C.-H. Wang, and C. H. Chen, “Compact microstrip bandpass filters with good selectivity and stopband rejection,” *IEEE Trans. Microw. Theory Tech*., vol. 54, no.2, pp. 533-539, Feb. 2006.

[24] First Report and Order in the matter of Revision of Part 15 of the Commission’s Rules Regarding Ultra-Wideband Transmission Systems, Released by Federal Communications Commission ET-Docket 98-153, Apr. 22, 2002.

[25] T. G. Ma and S. K. Jeng, “Planar miniature tapered-slot-fed annular slot antennas for ultra-wideband radios,” *IEEE Trans. Antennas Propag*., vol. 53, pp. 1194–1202, Mar. 2005.

[26] N. Behdad and K. Sarabandi, “A multiresonant single-element wideband slot antenna,” *IEEE Antennas Wireless Propag. Lett*., vol. 3, pp. 5–8, Jan. 2004.

[27] C. Y. D. Sim, W. T. Chung, and C. H. Lee, “Compact slot antenna for UWB applications,” *IEEE Antennas Wireless Propag. Lett*., vol. 9, pp. 63–66, 2010.

[28] T.Yang and W. A. Davis, “Planar half-disk antenna structures for ultrawideband communications,” in *Proc. IEEE AP-S Int. Symp.*, Jun. 2004, vol. 3, pp. 2508–2511.

[29] N. P. Agrawall, G.Kumar, and K. P. Ray, “Wide-band planar monopole antennas,” *IEEE Trans. Antennas Propag*., vol. 46, no. 2, pp. 294–295, Feb. 1998.

[30] L. Jianxin, C. C. Chiau, X. Chen, and C. G. Parini, “Study of a printed circular disc monopole antenna for UWB systems,” *IEEE Trans. Antennas Propag*., vol. 53, no. 11, pp. 3500–3504, Nov. 2005.

[31] M. J. Ammann and Z.-N. Chen, “Wideband monopole antennas for multi-band wireless systems,” *IEEE Antennas Propag. Mag*., vol. 45, no. 2, pp. 146–150, Apr. 2003.

[32] M. J. Ammann and Z. N. Chen, “A wide-band shorted planar monopole with bevel,” *IEEE Trans. Antennas Propag*., vol. 51, pp. 901–903, Apr. 2003.

[33] C.-W. Ling, W.-H. Lo, R.-H. Yan, and S.-J. Chung, “Planar binomial curved monopole antennas for ultrawideband communication,” *IEEE Trans. Antennas Propag*., vol. 55, pp. 2622–2624, Sep. 2007.

[34] J. N. Lee and J. K. Park, "Impedance characteristics of trapezoidal ultra-wideband antennas with a notch function," *Microw. Opt. Technol. Lett*., vol. 46, no. 5, pp. 503–506, Sep. 2005.

[35] K. L. Wong, Y. W. Chi, C. M. Su, and F. S. Chang, "Band-notched ultra-wideband circular-disk monopole antenna with an arc-shaped slot," *Microw. Opt. Technol. Lett*., vol. 45, no. 3, pp. 188-191, May 2005.

[36] C. Y. Huang and W. C. Hsia, "Planar ultra-wideband antenna with a frequency notch characteristic," *Microw. Opt. Technol. Lett*., vol. 49, no. 2, pp. 316–320, Feb. 2007.

[37] H. Yoon, H. Kim, K. Chang, Y. J. Yoon, and Y. H. Kim, "A study on the UWB antenna with band-rejection characteristic," in *Proc. IEEE AP-S Int. Symp*., Jun. 2004, vol. 2, pp. 1784–1787.

[38] I. J. Yoon, H. Kim, K. Chang, Y. J. Yoon, and Y. H. Kim, "Ultra wideband tapered slot antenna with band-stop characteristic," in *Proc. IEEE AP-S Int. Symp*., Jun. 2004, vol. 2, pp. 1780–1783.

[39] S. Y. Suh, W. L. Stutzman, W. A. Davis, A. E. Waltho, K. W. Skeba, and J. L. Schiffer, "A UWB antenna with a stop-band notch in the 5-GHz WLAN band," in *Proc. IEEE ACES Int. Conf*., Apr. 2005, pp. 203-207.

[40] Y. Gao, B. L. Ooi, and A. P. Popov, "Band-notched ultra-wideband ring-monopole antenna," Microw. Opt. Technol. Lett., vol. 48, no.1, pp. 125-126, Jan. 2006.

[41] C.-Y. Hong, C.-W. Ling, I-Y. Tarn, and S.-J. Chung, "Design of a planar ultrawideband antenna with a new band-notch structure," *IEEE Trans. Antennas Propag*., vol. 55, pp. 3391–3397, Dec. 2007.

[42] S.-J. Wu, C.-H. Kang, K.-H. Chen, and J.-H. Tarng, "Study of an ultrawideband monopole antenna with a band-notched open-looped resonator," *IEEE Trans. Antennas Propag*., vol. 58, pp. 1890–1897, Jun. 2010.

[43] C. Quendo, E. Rius, and C. Person, "Narrow bandpass filters using dual-behaviors resonators," *IEEE Trans. Microw. Theory Tech*., vol. 51, no. 3, pp. 734-743, Mar. 2003.

[44] Z. Ma and Y. Kobayashi, "Design and realization of bandpass filters using composite resonators to obtain transmission zeros," in *Proc. 35th Eur. Microw. Conf*., 2005.

[45] C.-T. Chuang and S. J. Chung, "New printed filtering antenna with selectivity enhancement," in *Proc. 39th Eur. Microw. Conf.*, 2009, pp. 747-750.

[46] N. Yildirim *et al.*, "A revision of cascade synthesis theory covering cross-coupled filters," *IEEE Trans. Microw. Theory Tech*., vol. 50, no. 6, pp. 1536-1543, Jun. 2002.

[47] D. M. Pozar, *Microwave Engineering*, 3nd ed. New York: Wiley, 2005.

[48] AWR Microwave Office (MWO). AWR Corporation, Segundo, CA, 2010.

[49] H.-Y. Anita and K.-K. M. Cheng, "Novel dual-band planar resonator and admittance inverter for filter design and applications," in *IEEE MTT-S Int. Microw. Symp. Dig*., May 2005, pp. 2187-2190.

[50] W. L. Stutzman and G. A. Thiele, *Antenna Theory and Design*. New York: Wiley, 1998.

[51] High Frequency Structure Simulator (HFSS). Ansoft Corporation, Pittsburgh, PA, 2001.

[52] Yu-Shin Wang, Ming-Chou Lee, and Shyh-Jong Chung, "Two PIFA-Related Miniaturized Dual-Band Antennas," *IEEE Trans. Antennas Propagat*., Vol. 55, Issue 3, Part 2, pp. 805 – 811, Mar. 2007.

[53] M. Matsuo, H. Yabuki, and M. Makimoto, "The design of a half-wavelength resonator BPF with attenuation poles at desired frequencies," in *IEEE MTT-S Int. Microw. Symp. Dig*., 2000, pp. 1181-1184.

[54] G. L. Matthaei, L. Young, and E. M. T. Jones, *Microwave Filters, Impedance-Matching Network, and Coupling Structures*. Norwood, MA: Artech House, 1980.